Multiplexed and reproducible high content screening of live and fixed cells using the Dye Drop method

Caitlin E. Mills[1*], Kartik Subramanian[1,2*], Marc Hafner[1,3*], Mario Niepel[1,4], Luca Gerosa[1,3], Mirra Chung[1], Chiara Victor[1], Ben Gaudio[1], Clarence Yapp[1], Peter K. Sorger[1]

* These authors contributed equally

1 Laboratory of Systems Pharmacology, Department of Systems Biology, Harvard Medical School, Boston, MA 02115

2 Current address: Bristol Myers Squibb, Cambridge, MA 02142

3 Current address: Genentech, Inc., South San Francisco, CA 94080

4 Current address: Ribon Therapeutics, Inc., Cambridge, MA 02140

Correspondence email: peter_sorger@hms.harvard.edu

ORCiD:
Caitlin E. Mills: 0000-0002-2608-4084
Kartik Subramanian: 0000-0002-6900-8882
Marc Hafner: 0000-0003-1337-7598
Mario Niepel: 0000-0003-1415-6295
Luca Gerosa: 0000-0001-6805-9410
Mirra Chung: 0000-0002-4033-7930
Chiara Victor: 0000-0002-9002-1328
Ben Gaudio: 0000-0002-7003-5052
Clarence Yapp: 0000-0003-1144-5710
Peter K. Sorger: 0000-0002-3364-1838

ABSTRACT

High throughput measurement of cell perturbation, by libraries of small molecules or gene knockouts, is a key step in functional genomics and pre-clinical drug development. However, it is difficult to perform viable, single-cell assays in 384-well plates, limiting many studies to simple well-average measurements (e.g. CellTiter-Glo®). Here we describe a public domain "Dye Drop" method in which sequential density displacement is used to perform multi-step assays for cell viability and EdU incorporation followed by immunofluorescence imaging. The method is rapid, reproducible, can be readily customized, and is compatible with either manual or automated laboratory equipment. We demonstrate Dye Drop in the collection of dose-response data for 67 drugs in 58 breast cancer cell lines and separate cytostatic and cytotoxic responses, thereby providing new insight into the effects of specific drugs on cell cycle progression and cell viability. Dye Drop substantially improves the tradeoff between data content and cost, enabling collection of large information-rich datasets.

INTRODUCTION

Accurate measurement of cellular responses to perturbation – genetic and drug induced – is integral to studying regulatory mechanisms and developing new therapies. In the case of small molecules, dose-response studies are increasingly performed on a relatively large scale using panels of genetically diverse cell lines and compound libraries.[1,2] Six to nine point dose-response curves are considered the standard for in-depth analysis for drugs.[3] When necessary technical and biological repeats are included, a pre-clinical pharmacology experiment on an ~50 cell line panel can require assaying 10^4 to 10^5 individual conditions (30 to 300 384-well plates), which is similar in scale to a primary high content compound screen using diversity libraries or whole-genome screening with RNAi or CRISPR-Cas9 libraries.[4] A key difference is that the vast majority of the data points in a profiling

experiment using a bioactive compound set or focused knockout collection (e.g, of a gene family) contribute to the final dataset whereas only a small number of hits are typically pursued from chemical diversity or genomic screens. Profiling studies therefore require sensitive, reproducible assays.

To increase throughput, cell-based small molecule screens are often performed using a single, relatively simple readout such as well-average ATP levels (measured in lysate),[5] a reasonable but far from perfect surrogate for cell viability.[6,7] However, multiplexed assays that extract more information from each condition provide superior insight into mechanism, making follow-up studies more efficient; multiplexed screening also promises to better identify cell types and disease states in which a small molecule might have the greatest therapeutic potential.[8] This has led to increasing use of high content screening, which is commonly based on fluorescence microscopy. For example, "cell painting" (five-channel, high resolution, multiplexed imaging of fixed cells) has made single-cell morphological measurements feasible at scale.[9] Live-cell assays have additional advantages since they yield detailed information about cell to cell heterogeneity and response dynamics.[10,11]

In any screen, fundamental tradeoffs exist between throughput, number of measurements per condition, cost, and reproducibility; this is true for systematic screening of cell and drug panels as well as genome-scale screens. Mix-and-read assays, CellTiter-Glo® in particular, are popular because they are rapid and simple to perform whereas live-cell imaging is much less common because it requires specialized expertise, instrumentation, and data analysis methods. However, any attempt to optimally balance simplicity and cost with high information content must consider the substantial effort and expense of maintaining panels of mammalian cell lines and setting up a multi-drug dose response experiment (personnel, time, media, multi-well plates, drug treatments etc.). Accuracy and reproducibility are also essential:[12] the public release of large scale drug-response data has been marred by controversy arising from poor agreement between different databases.[13,14] We have studied the

underlying issues[15] and concluded that much of the problem arises from inherent differences between cell lines that are not adequately accounted for in assay design. Failure to consider the impact of differences in cell proliferation rates makes a particularly large contribution to inconsistencies.[16]

Another common technical contributor to irreproducibility in high content live-cell or immunofluorescence assays performed in multi-well plates is uneven loss of cells[17], particularly those that are dying or undergoing mitosis (both of which are less adherent than interphase cells). The extent of loss varies with cell type, perturbation, type of assay and operator.[15] In search of a simple and robust solution to this problem we found that a wide variety of assays could be performed on live and fixed cells with retention of fragile subpopulations by performing multi-step procedures using a sequence of solutions each made slightly denser than the last by addition of iodixanol (OptiPrep™), an inert liquid used in radiology. This effectively eliminates the need for mix and wash steps.[18] Multi-channel pipettes are used to add each solution needed for an assay along the edges of wells in a multi-well plate so that the solution "drops" gently to the bottom of the well, displacing the previous solution with high efficiency and minimal mixing (testing with vital dyes yielded the "Dye Drop" moniker). As a practical matter, we found that once cells are fixed, conventional washing can be performed and that density-based displacement is therefore most critical for live cell assays and fixation steps. However, the Dye Drop procedure has the benefit at all stages of an experiment of keeping reagent costs to a minimum because the volume needed for each step is several-fold lower than with conventional procedures.

In this paper, we describe development, testing and use of minimally disruptive, customizable, microscopy-based "Dye Drop" and "Deep Dye Drop" assays that use sequential density displacement to optimally collect multiplexed data at low-cost with high reproducibility. We describe several different ways to implement Dye Drop assays to obtain detailed cell cycle information and to quantify single-cell phenotypes that are obscured by population-average assays (e.g. formation of DNA repair foci). Dye

Drop methods are an ideal complement to the growth-rate (GR) inhibition method of computing dose responses[15,19,20] and when combined, greatly improve the depth and accuracy of data while only slightly increasing cost. They can also be used as an entry point for high-plex immunofluorescence, by CyCIF for example.[21] We expand on the GR framework to make it possible to distinguish cytotoxic and cytostatic drug effects based on Dye Drop data and we generate a large-scale Dye Drop dataset using a panel of breast cancer cells and a kinase inhibitor library. This has allowed us to develop and test a complete pipeline of public domain tools, open-source software and exemplary results for performing high throughput, multiplexed dose-response and screening studies in cell lines.

RESULTS

Dye Drop assays provide accurate measurements of cell viability in multi-well plates

Errors and irreproducibility in experiments involving adherent cells grown in multi-well plates have four primary causes: (i) patterned (systematic) biases that arise from edge effects and unequal local growth conditions across a plate; (ii) disturbance and loss of some, but not all, cells in a well due to differences in properties, notably adhesion; (iii) incomplete exchange of reagents during washing steps due to the use of small volumes and high surface tension; and (iv) inadequate or incorrect data processing.[15,22,23] These factors often interact; for example, high flow rate or agitation during wash or media-exchange steps disturb dying, mitotic and weakly adherent cells whereas gentle methods can result in insufficient liquid exchange. Several of these problems become worse as wells become smaller and liquid volumes decrease (e.g. 384 vs 96 well plates).[24] We, and others, have previously described how systematic bias can be mitigated through sample randomization, use of humidified secondary containers etc.[15,25]

In the current work we focus on errors introduced by unpredictable cell loss and uneven reagent exchange encountered in performing multi-parameter assays on live and fixed cells in 384 well assay

plates. Specifically, we sought an approach to assaying live cells in multi-well plates that optimized the following factors: (i) simplicity, low cost and use of common commercially available reagents; (ii) minimal disturbance and good retention of delicate and poorly adhered cells; (iii) compatibility with vital (live-cell) assays to enable measurement of viability, DNA incorporation, and cell cycle progression; (iv) simple customization to enable measurement of proteins and phenotypes relevant to a specific biological problem under investigation; and (v) compatibility with simple robots and manual multichannel pipettes. Preliminary studies established that many assays could be performed in the presence of OptiPrep™.[26] Multi-step procedures are performed using a series of solutions, each made denser than the last by addition of OptiPrep™ so that successive solutions flow to the bottoms of wells, displacing the previous solution without aspiration or mixing and without disturbing fragile cells.

To test Dye Drop methods, we measured drug-induced growth arrest and cell death using live cell microscopy followed either by a standard wash and fixation, or fixation using an OptiPrep™-containing solution. Live cell microscopy of MCF 10A cells expressing H2B-mCherry made it possible to monitor proliferation and death at single-cell resolution in a time-resolved manner without any fixation or wash steps and served as a control for development of Dye Drop methods. Cells were exposed for 24 h to four cytotoxic drugs (dinaciclib, paclitaxel, staurosporine, and vincristine) at nine doses spanning four orders of magnitude. The YOYO-1 vital dye was added to the medium to detect dead and dying cells and imaging was performed on a microscope with an environmental control chamber equipped to handle microtiter plates. When live-cell acquisition was complete, a minimal Dye Drop procedure was performed by fixing cells with 4% formaldehyde in 10% OptiPrep™ in PBS followed by aspiration, addition of PBS and repeated imaging of the now fixed cells. We found that viability dose-response curves for each drug recorded pre- and post-fixation with OptiPrep™ were indistinguishable (**Fig. 1a**). In contrast, when live cell imaging was followed by conventional washes

using an automated plate washer and then fixation, we found that the number of cells per well fell following each wash (**Fig. 1b, Supplementary Fig. 1a**) and that the magnitude of the effect was drug dependent; we have previously shown that condition-dependent assay variability is a primary contributor to data irreproducibility.[15] To show that OptiPrep™ did not affect cell proliferation at concentrations needed for live-cell assays, we added it to cells at concentrations up to 25% for one hour (**Supplementary Fig. 1b**), or at concentrations up to 5% for 24 h (**Supplementary Fig. 1c**) and then counted cells. Neither a pulsed exposure to a high concentration nor prolonged exposure to a lower concentration had any detectable effect on cell viability, consistent with literature describing the use of OptiPrep™ in density gradient purification of cells.[27] We conclude that Dye Drop fixation preserves cells vulnerable to loss from successive wash cycles and improves the accuracy of cell viability assays.

As an alternative to using CellTiter-Glo® or other luminescence-based assays to estimate well-average cell viability, we performed single-cell viability measurements using the Invitrogen Molecular Probes LIVE/DEAD assay. The amine-reactive and fixable LIVE/DEAD dye (LDR) was combined with Hoechst 33342[28] by suspending both in 10% OptiPrep™ in PBS and then adding the solution to wells with a multichannel pipette, thereby displacing the growth medium. Following a 30 min incubation, a solution containing 20% OptiPrep™ and 4% formaldehyde was used to displace the LDR and Hoechst dyes and to fix the cells (see online Methods for details; **Supplementary Fig. 1d-e**). Once fixed, even weakly adhered cells were resistant to washing, allowing a variety of staining protocols to be followed, as described below

Deep Dye Drop assays provide multiplexed cell viability and cell cycle measurements

To study the effects of chemical or genetic perturbation on the cell cycle, including rate of division and DNA replication, arrest at discrete cell cycle stages, induction of polyploidy, etc., we integrated a live-cell EdU incorporation assay into the Dye Drop method. EdU was added to cells at the

same time as the LDR viability dye (but without Hoechst 33342) resulting in incorporation by cells actively replicating DNA. Following fixation, EdU incorporated into DNA was labeled using Click chemistry to visualize S-phase cells; M-phase cells were stained with an anti-phospho-histone H3 antibody (anti-pH3; available fluorophonre-conjugated, avoiding the need for secondary antibodies) (**Fig. 1c-f**). Incubating cells in the presence of antibody overnight resulted in good quality staining and provided a natural break-point in the protocol; Hoechst 33342 staining was performed in parallel. Imaging of cells processed this way generated the classic "horseshoe" profile of DNA synthesis and content,[29] enabling detailed analysis of DNA replication rates and S-phase errors; it also reliably discriminated G1 and G2 populations and detected aberrant DNA content (**Fig. 1g-h, Supplementary Fig. 1f**). Moreover, the now-fixed plates could be subjected to a series of additional staining protocols with the option of using either the Dye Drop approach to economize on reagents or switching to conventional plate washing methods.

Customizing Dye Drop assays for different endpoints

To customize the Deep Dye Drop method for different biological endpoints we tested a range of antibodies (**Fig. 2a-e**) and found that it was straightforward to acquire data on cell cycle state and viability in living cells as described above and then perform immunofluorescence on fixed cells. For example, when MCF7 cells treated with the CDK4/6 inhibitor palbociclib were assayed using Deep Dye Drop and an antibody against phospho-pRb, we could measure dose-dependent target engagement at a single cell level (drug pharmacodynamics; **Fig. 2a**) along with progressive G1 arrest. When cells were additionally stained with an anti-beta-actin antibody, a change in cell size was readily detectable (**Fig. 2b**).[30,31] Similarly, when MCF 10A cells were treated with the topoisomerase II inhibitor, etoposide and stained with anti-53BP1 antibody, the fraction of cells with multiple 53BP1-containing DNA damage foci increased in a dose dependent manner (**Fig. 2c**). In this case we used an anti-mouse secondary

antibody to show that Deep Dye Drop is not limited to fluorophore-conjugated antibodies. Finally, when MCF7 cells were treated with actinomycin D, mitochondrial outer membrane permeabilization (MOMP), a key step in commitment to apoptosis[32] could be quantified based on changes in cytochrome C localization (**Fig. 2d**). Thus, given a suitable antibody for immunofluorescence, Deep Dye Drop assays can be used to measure many molecular processes at a single cell level in normally growing and perturbed cells.

Most modern fluorescence microscopes are equipped to measure five or more fluorescent channels. To develop a five-channel Deep Dye Drop protocol, we performed dual antibody staining and identified five complementary and commercially available assays that could readily and reproducibly be performed in a 384 well format: (i) LIVE/DEAD assessment (ii) live-cell EdU incorporation (iii) counting of fixed cells, in combination with DNA content and morphology in the Hoechst channel and (iv-v) two channels of immunofluorescence using Alexa 488 and Alexa 750-conjugated primary or secondary antibodies (anti-pH3 and anti-53BP1 primary antibodies were used in **Fig. 2e,** but antibody selection should be based on the questions being pursued).

To determine if Deep Dye Drop is compatible with highly multiplexed florescence imaging, we performed cyclic immunofluorescence (CyCIF),[33] a method that collects 10-20 plex data through sequential rounds of 3 or 4-plex antibody staining, imaging, and fluorophore oxidation. We found the two approaches to be compatible (**Fig. 3a**) but that it was necessary to quench the copper in the click chemistry used for EdU labeling prior to addition of the hydrogen peroxide-containing fluorophore inactivation solution. Quenching can be performed using EDTA (see Methods), or alternatively, the click reaction can be performed after all CyCIF staining cycles are complete. To illustrate the integration of Dye Drop assays with CyCIF, we treated MCF7 and MCF 10A cells with ribociclib, BMS-265246 or DMSO for 72 h, performed Deep Dye Drop staining and then three rounds of CyCIF staining. We

visualized the multiplexed single cell CyCIF data in UMAP space and found that MCF7 and MCF 10A cells clustered separately, as did each condition tested (**Fig. 3b**; note that 10 μM BMS-265246 is cytotoxic and there are far fewer cells remaining under these conditions). A combination of Deep Dye Drop and CyCIF makes a wide range of phenotypic assays available, and it is possible to introduce a gap of up to several weeks (after plates are fixed) between the initial live-cell assays and CyCIF so that preliminary data can inform and focus assay choice for detailed analysis of key parameters.

Rapid adaptation of tumor cells to drug is a barrier to successful therapy and an area of intense focus in pre-clinical research.[34] To illustrate the use of Dye Drop to assay in a measurement of time-dependent GR values , we exposed hormone receptor positive (HR^+) MCF7 cells to three related CDK4/6 inhibitors approved to treat $HR^+/HER2^-$ breast cancer (palbociclib, ribociclib, and abemaciclib).[35,36] Proliferation was inhibited for 24 hours after drug exposure, but a subset of cells escaped inhibition (4.4 % at 1 μM after 72 h) at all concentrations of palbociclib and ribociclib tested, with an inverse dose-dependence (**Fig. 3c-e**). Abemaciclib was the most effective drug at preventing cell cycle re-entry, likely due to its inhibition of targets other than CDK4 and CDK6[37] (**Fig. 3c-e** and inset plots). This example is illustrative of the advantages of collecting single-cell data, as opposed to more common well-average measurements, particularly when only a subset of the cells in a well are involved in a phenomenon of interest; this commonly includes time-dependent emergence of drug-adapted cells as well as other forms of drug resistance.[38]

Using Dye Drop to systematically screen small molecule drugs in breast cancer cell lines

To demonstrate the use of Dye Drop assays at scale, a panel of 58 breast cancer cell lines was exposed to a library of 67 approved and investigational kinase inhibitors and other small molecules. The panel included multiple non-malignant breast epithelial lines (labeled NM) and many lines routinely used to study the three major breast cancer subtypes: hormone receptor positive (HR^+), HER2 amplified

or overexpressing ($HER2^{amp}$), and triple negative (TNBC; which lack expression of estrogen, progesterone and HER2). Responses were measured 72 h after addition of drug at nine concentrations spanning a 10^4 dose range (plus DMSO-only negative controls). All assays were performed in triplicate or quadruplicate to measure technical repeatability. This yielded a total of ~3,900 nine-point dose response curves computed from ~116,000 wells (~35,000 unique conditions) with each well yielding data on ~0.5 to 15 $x10^3$ single cells (**Fig. 4a, Supplementary Fig. 2**).

GR values were determined for each drug, dose and cell line based on the number of viable cells at t = 0 h and 72 h followed by curve-fitting to estimate four drug response metrics:[16] (**Fig. 4b**): (i) potency, as measured by GR_{50}, the drug concentration at which GR = 0.5, or GEC_{50}, the concentration at half-maximum effect (relevant when GR = 0.5 is not reached); (ii) efficacy, as measured by the maximum drug effect, GR_{max}; (iii) the slope of the fitted dose response curve, h_{GR}, and (iv) the area over the GR curve GR_{AOC}.[39–41] Drug response data exhibited good reproducibility (median standard deviation of GR values = 0.07 and median coefficient of variation ~11%) and recapitulated clinical evidence. For example, PIK3CA-kinase domain mutant lines were significantly more sensitive than PTEN low lines to alpelisib (PIQRAY®, approved for PIK3CA-mutant HR+/HER2- advanced and metastatic disease; 2-way ANOVA P-value < 0.05),[42] $HER2^{amp}$ lines were sensitive to neratinib (NERLYNX® approved for $HER2^{amp}$ disease; 2-way ANOVA P-value < 0.01)[43], luminal lines were more sensitive than basal lines to everolimus (AFINITOR® approved for HR+ disease; two-tailed unpaired t-test P-values < 0.001)[44] and pRb-deficient lines were resistant to CDK4/6 inhibitors palbociclib, ribociclib and abemaciclib (IBRANCE®, KISQALI®, and VERZENIO®; two-tailed unpaired t-test P-values < 0.001) (**Fig. 4c**; see **Supplementary Fig. 3a** for all others). Several additional drugs exhibited subtype specificity that matched their targeted clinical indication: relative to other subtypes, HR^+ cell lines were more sensitive to the AKT inhibitors AZD5363 and ipatasertib, and

mTOR inhibitors everolimus, AZD2014 and LY302341; TNBC cell lines were more sensitive to the WEE1 inhibitor adavosertib, the ATR inhibitor AZD6738, and the PARP inhibitors rucaparib and olaparib.[45–47]

One striking feature of these data is that NM lines were not more resistant overall than cancer lines; this was true of pre-clinical compounds and drugs approved by the FDA for treatment of breast cancer (**Fig. 4c**, in bold). NM cells were actually more sensitive than tumor cells as a whole to the ERK1/2 inhibitor BVD523, and to the MEK1/2 inhibitor trametinib (two-tailed unpaired t-test, P-value < 0.05). This is not a new observation[48] but suggests that even systematic drug studies involving cultured breast cancer cells are unlikely to identify a therapeutic window between NM and cancer lines.

Distinguishing cytostatic and cytotoxic drug effects

A value of GR = 1 corresponds to unperturbed proliferation resulting in identical numbers of viable cells in drug-treated and control cultures; GR = 0 corresponds to no increase in viable cell number; and GR < 0 to net cell loss. The GR = 0 condition can arise because all cells in the culture arrest in a viable state (true cytostasis) or because the number of cells that die equals the number born over the duration of the assay. To distinguish these possibilities, we compared the fraction of dead cells to GR values across all drugs, concentrations, and cell lines (**Fig. 4d**). We observed the expected negative correlation but with high dispersion around the trend line: at GR = 0, the fraction of dead cells varied from 0 to 48% (median = 12%). By comparing the drug-induced change in S-phase and dead cell fractions (for $-0.1 < GR < 0.1$), we found that birth and death balanced (S-phase and death fractions within 5% of each other) in only ~44% of conditions. The ~24% of conditions with high cell death but low S-phase fraction (i.e. when the difference was >10%) likely represent delayed-onset cell killing whereas low cell death with high S-phase fraction likely reflects adaptation (~7% of conditions) (**Fig. 4e**). In such cases the underlying assumption in GR calculations that growth rate is constant is violated

and time-dependent GR measurements are required (**Fig. 3c-e**). We noted two caveats in these data. First, a fraction of cells undergoing programmed cell death lyse completely and are therefore not captured as LDR-positive in the "dead cell count" (generally, conditions with GR ~ -1.0 exhibit the greatest lysis). Additionally, a fraction of cultured cells die in the absence of drug treatment (median value 5%; range ~1 – 19%). To account for these effects, drug efficacy should be based on both dead cell count and the fraction of viable cells (i.e. GR value) and cell death should be reported as the drug-induced increase over baseline. These limitations do not weaken our conclusion that at GR = 0 true cytostasis is less common than balanced birth and death; if anything, lysis of dead cells leads to an underestimate of the extent of cell killing.

To better distinguish between cytostasis and cytotoxicity we used an ordinary differential equation (ODE) model of proliferation to estimate rates at which cells transition from proliferation into stasis (k_s) or death (k_d) (see Methods). We then computed dose-response curves and metrics for cytostatic and cytotoxic responses (GR^S and GR^T; note that overall GR value is not mathematically equal to the sum of GR^S and GR^T but approximately to their product, see methods; **Fig. 4f**, **Supplementary Fig. 3b**). With data comprising only two time points, the model necessarily assumes that k_s and k_d are constant over the course of the experiment. Taking the response of the $HER2^{amp}$ AU-565 cell line to neratinib as a case study, we found that it was well fit by a sigmoidal curve (h_{GR} = 0.84) and exhibited high potency (GR_{50} = 1.2 nM , GEC_{50} = 3.0 nM) and efficacy (GR_{max} = -0.70) (**Fig. 4a-b**). When the response was decomposed, the cytostatic component was 40-fold more potent (GEC^S_{50} = 1.1 nM) than the cytotoxic component (GEC^T_{50} = 48 nM), but both were within the range of serum C_{max} in humans[49] (**Fig. 4h**). In support of these data, EdU incorporation exhibited half-maximal inhibition of DNA synthesis at 1.5 nM, consistent with a requirement for HER2 in cell cycle progression[50] and LDR data confirmed half-maximal cell killing at ~30 nM (**Supplementary Fig. 4**).

Across all drugs and cell lines toxicity as measured by GR^T_{max} and potency as measured by GEC^S_{50} varied widely (GR^T_{max} = 0.06 to -0.74 and GEC^S_{50} median = 0.49 μM, interquartile range (IQR) = 4.85 μM) and their correlation (Spearman r = 0.41, P-value < 0.001) masked substantial differences by drug type (**Fig. 5a; Supplementary Fig. 3b**). For example, palbociclib and ribociclib and the CDK4/6-targeting PROTAC (PROteolysis TArgeting Chimera; a drug that induces proteasome-mediated degradation of a target),[51] BSJ-03-124 varied in potency (GEC^S_{50}, median = 0.54 μM IQR = 8.2) across cell lines but induced little or no cell death (GR^T_{max} ~ 0). In contrast, dinaciclib and alvocidib, which target multiple CDKs (i.e. CDK1/2, CDK4/6, CDK5, 7, 9) differed primarily in toxicity (GR^T_{max}= 0 to -0.7 for both). Finally, abemaciclib[37] and BSJ-03-123 (CDK6 PROTAC),[52,53] compounds that have multiple targets varied on both potency and efficacy axes. A similar pattern was observed for the CDK7 inhibitor YKL-5-124, which varied in potency and efficacy whereas less selective inhibitors with activity against CDK12/13 such as THZ1 (CDK7/12/13) and THZ531 (CDK12/13) varied primarily in cytotoxicity. Thus, deconvolution of Dye Drop dose-response data can discriminate modes of anti-cancer drug action and reveal differences in drug dose-response relationships (**Fig. 5b**). The impact of these differences on clinical efficacy will need further study but we note that drugs with little variation in potency, such as dinaciclib and alvocidib, failed in trials due to excess toxicity, whereas drugs such as abemaciclib varying on both potency and efficacy axes may be superior to drugs that induce little or no cell killing, such as ribociclib.[37,54]

Pre-treatment cell cycle distributions and drug-induced cell cycle effects

Deep Dye Drop data reveal great diversity in cell cycle distribution across cell lines before and after drug exposure. At baseline, G1 fraction varied from 15% to 86%, G2 fraction from 6% to 40%, and S phase fraction varied from 4% to 63%; G1 and S phase fractions significantly correlated with division rate (Spearman r = -0.58 and r = 0.56, respectively; P-values < 0.001; **Supplementary Fig. 5a-b**).

Growth rates, as measured in DMSO-only cultures varied ~7-fold (from 17 h to 114 h per doubling) with HER2^{amp} lines (median growth rate 0.33 doublings/day) the slowest and NM cells the fastest (median 0.95 doublings/day) (**Fig. 6a**). This wide range of division times, a known confounder in comparative studies based on relative viability metrics such as IC50 or AUC, highlights the importance of using GR metrics or similar methods to mitigate growth rate bias.[19,20]

We found that drug-induced changes in the G1, S and/or G2 fractions were dependent on the drug and cell line: a decrease in GR from 1 to 0 (net arrest) was most strongly associated with a reduction in S-phase cells (Spearman r = 0.57, P-value < 0.0001) and accumulation of cells in G1 or G2 (**Fig. 6b**). The CDK4/6 inhibitors ribociclib and abemaciclib shifted cell cycle distribution from S phase to G1 reflecting inhibition of the G1/S transition[37] whereas BMS-265246, a drug primarily targeting CDK1/2[55] induced G2 arrest (**Fig. 6b, Supplementary Fig. 5c-d**). Replication stress is a characteristic of cancer cell lines that can extend S phase and results in sensitivity to DNA damaging agents.[56] When we compared S-phase duration to division time for all cell lines, a subset of HR^{+} and TNBC cells had S-phases longer than 20 h (**Fig. 6c,** red dashed box). TNBC cells with extended S phases were enriched (as compared to all other TNBC lines, effect size > 2, t-test P-value < 0.05) in the expression of genes such as PKD1, a marker of poor metastasis-free survival[57] (**Fig. 6d**) and MVP, which is linked to chemoresistance;[58] GSEA revealed upregulation of '*Wnt-activated receptor activity*' (GO:0042813) and '*sphingosine-1-phosphate receptor activity*' (GO:0038036) (**Supplementary Table 1**) in these cells. Dysregulation of Wnt signaling is common in TNBC[59] and both WNT and sphingosine-1-phosphate pathways are implicated in metastasis.[55] When we examined the correlation between S-phase duration (in the absence of drug) and GR_{max}, we observed significant correlation for AZD6738, an inhibitor of ATR, a kinase that detects and responds to replication stress (Spearman r = 0.44, P-value = 0.03), adavosertib, an inhibitor of the G2/M checkpoint kinase, WEE1 (Spearman r = 0.39, P-value = 0.05) and

with three inhibitors (BSJ-01-175 Spearman r = 0.49, P-value = 0.01; THZ1 Spearman r = 0.39, P-value = 0.01; and THZ531 Spearman r = 0.32, P-value = 0.1) that target CDK12/13 a known regulator of DNA damage repair and Wnt pathway genes[61] (**Fig. 6e, Supplementary Fig. 5e**). In aggregate these data strongly suggest that differences in baseline and drug-induced cell cycle states readily measured by Deep Dye Drop assays are associated with features important for the biology and treatment of breast cancer.

DISCUSSION

The Dye Drop method described here constitutes a flexible and extendable set of protocols for efficiently performing high throughout viable- and fixed-cell assays in multi-well plates. By adding as little 15 µl per well (for a 384-well plate) of each of a series of increasingly dense solutions, reproducible high-throughput data can be obtained from widely used viable-cell LIVE/DEAD and EdU incorporation assays. Small assay volumes and compatibility with existing reagents lower barriers to use including cost. Both manual multi-channel pipettes and automated reagent dispensers can be used in Dye Drop, and once cells are fixed conventional plate washing is possible. By coupling Dye Drop with multiplexed imaging (e.g. using CyCIF),[62] 10-15 single-cell measurements can be performed on each well at only slightly higher cost than conventional CellTiter-Glo® assays. For medicinal chemistry campaigns or annotation of known bioactive collections (for which response rates are high), Deep Dye Drop yields a substantially more favorable balance between throughput, information content and cost than current approaches. For large-scale, low hit-rate screens of small molecule, siRNA, or CRISPR-Cas9 libraries, it is likely to be more efficient to perform a minimal Dye Drop protocol in the first round and re-screen hits in a second round of high-plex Deep Dye Drop assays.

The use of standardized data analysis pipelines is essential for ensuring the accuracy and reproducibility of multi-parametric single-cell assays.[15] We have therefore developed a set of

computational routines for designing and performing drug dose-response assays using the Dye Drop method (**Supplementary Fig. 6**, see online Methods). These routines are integrated with scripts we previously developed for computing GR metrics[63] in a single tool box. Dye Drop dose-response analysis features a series of "flags" that alert users when experimental design criteria and results such as the number of controls, the dose range, and the accuracy of curve fitting are suboptimal.

By measuring the responses of a panel of breast cancer lines to a collection of small molecule drugs we have demonstrated the feasibility of Dye Drop at scale. We find that breast cancer lines vary substantially in proliferation rates in the absence of drug and in distribution through cell cycle phases. Non-malignant cells are the fastest growing on average and $HER2^{amp}$ cells the slowest (non-malignant cells also have the lowest rates of cell death in the absence of drug, median ~2%). G1 and S-phase are the most variable across lines. The origins of this variability are yet to be identified, but likely to arise from recurrent mutations in genes that ensure the fidelity of DNA synthesis and repair (e.g. p53 and BRCA1/2) and the consequent replication stress.[56] Subtype-specific differences in growth rate also make clear that to avoid confounding drug response and proliferation rate, it is essential to normalize responses using GR metrics or similar approaches. With this normalization biomarkers used clinically (e.g. HER2, PTEN status) do reproduce in cell line panels but non-malignant cells are very rarely more resistant to approved and investigational anti-cancer drugs than cancer cells and are not less prone to cell death; thus, these should not be criteria in pre-clinical drug screens.

Counting viable cells or measuring a well-average surrogate such as ATP level (e,g. using CellTiter-Glo®) does not distinguish cell cycle arrest (cytostasis) from cell killing (cytotoxicity). Using a simple model and Dye Drop data it is possible to make such a distinction and uncover dramatic differences by cell line and drug. Some drugs — the FDA-approved CDK4/6 inhibitors, ribociclib and palbociclib for example — differ widely in potency across a cell line panel but elicit little or no cell

killing. In contrast, drugs such as the CDK1/2/5/9 inhibitor dinaciclib (whose clinical development ended in phase 2), have nearly the same potency in all cell lines and differ instead in cytotoxicity. Drugs such as abemaciclib differ in both potency and efficacy.[64] The origins of these differences are not yet known, but abemaciclib may be the most clinically active of the approved CDK4/6 inhibitors[65] whereas dinaciclib and alvocidib[66] are associated with serious toxicity in humans. We speculate that variation in both efficacy and potency, as exhibited by abemaciclib or the tool compound YKL-5-124 may be a property of an ideal cancer therapeutic.

METHODS

Cell culture

Cell lines were maintained in their recommended growth medium and culture conditions as detailed in **Supplementary Table 2**. Conventional cell lines were identity verified by STR profiling, and newly established cell lines were STR profiled to ensure they were unique and to set benchmarks for future reference.

Screening

Drugs were arrayed in nine-point half-log dilution series in 384 well library plates (**Supplementary Table 3**). The identity and purity of the drugs were verified by LC-MS. Each daughter plate contained 10 µl per well, and was thawed a maximum of 12 times. Cells were seeded in 384 well CellCarrier or CellCarrier ULTRA plates (Perkin Elmer, Waltham, MA) with a multidrop combi liquid dispenser at the densities listed in **Supplementary Table 2**, and allowed to adhere for 24-36 hours prior to drug treatment. Drugs were delivered from library plates via pin transfer with a custom E2C2515-UL Scara robot (Epson, Long Beach, CA) coupled to stainless steel pins (V&P Scientific, San Diego, CA) at the ICCB-Longwood Screening Facility, or from stock solutions with a D300 digital drug dispenser

(Hewlett-Packard, Palo Alto, CA). At the time of drug delivery, replicate plates were stained and fixed to serve as time=0 reference data for GR-based calculations, and 72 hours later treated plates were stained and fixed according to the Dye Drop or Deep Dye Drop protocol (see below).

Dye Drop assay

Cells, in 384 well plates, were stained by adding 15 µl of a staining solution per well: 1 µg/ml Hoechst 33342 (Thermo Fisher, Waltham, MA) and 1:2000 LIVE/DEAD far red dye (LDR) (Thermo Fisher, Waltham, MA) in 10% OptiPrep™ (Sigma, St. Louis, MO) in PBS (Corning, Glendale, AZ). After thirty minutes at room temperature (RT), cells were fixed by adding 20 µl of 4% formaldehyde (Sigma, St. Louis, MO) in 20% OptiPrep™ in PBS per well and incubating for 30 minutes. After fixation, the wells were aspirated and filled with 80 µl PBS, plates were sealed with foil adhesives (BioRad, Hercules, CA) and stored at 4˚C until imaged. A 16-channel automatic multi-pipette was used for the addition of the stain and fix solutions, all aspirate steps and other dispense steps were performed with an EL406 washer equipped with a 96-channel head (Biotek,Winooski, VT).

Deep Dye Drop assay

15 µl of a 10% OptiPrep™ solution in PBS containing 10 µM EdU (Lumiprobe, Waltham, MA) and 1:2000 LDR was added cell in each well of a 384 well plate and incubated for one hour at 37˚C. Cells were then fixed in 20 µl/well 4% formaldehyde in 20% OptiPrep™for 30 minutes at RT. The duration of the EdU pulse can be adjusted depending on the division time of the cell line or on the experimental conditions, however, in our experience a one-hour pulse of EdU at 37°C is sufficient for most conventional cell lines. Following fixation, the wells were aspirated using an EL406 washer. 15 µl of cell permeabilization solution, 0.5% Triton-X100 (Sigma, St. Louis, MO) in 10% OptiPrep™, was then added per well at room temperature (RT) followed, 20 minutes later, by 20 µl of Click chemistry solution (2 mM copper sulfate, 4 µM Sulfo-Cy3 azide (Lumiprobe, Waltham, MA), 20 mg/ml ascorbic

acid) in 20% OptiPrep™ to fluorescently label the incorporated EdU. After 30 minutes at RT, once the Click reaction was complete, the wells were aspirated, and 40 µl of Odyssey blocking buffer (LI-COR Biosciences, Lincoln, NE) was added per well for a minimum of one hour at RT, or up to overnight at 4°C to block the cells for immunofluorescence labeling. Next, an Odyssey blocking buffer solution containing 10% OptiPrep™ and 1:2000 Alexa 488-conjugated anti-phospho-histone H3 (S10) antibody (pH3) (clone D2C8, Cell Signaling Technology, Danvers, MA) to label M-phase cells and 2 µg/ml Hoechst 33342 to stain all nuclei, was dropped onto the cells and incubated overnight at 4°C. The overnight incubation ensures that the Hoechst staining saturates enabling accurate, image-based quantitation of DNA content. Post incubation, the plates were washed once with 0.01% PBS-Tween (Thermo Fisher, Waltham, MA) and twice with PBS, leaving a final volume of 80 µl of PBS in each well. The plates were then sealed with foil adhesives (BioRad, Hercules, CA) and kept at 4°C until imaged. As above, a 16-channel automatic multi-pipette was used for the addition of all stain and fix solutions, and all aspirate steps and other dispense steps were performed with an EL406 plate washer.

Microscopy and feature extraction

Image acquisition was performed with either an Operetta (Perkin Elmer, Waltham, MA) or an ImageXpress Micro-Confocal (IXM-C) (Molecular Devices, San Jose, CA) high throughput microscope using a 10x objective. Six fields of view per well were acquired with the Operetta, and four with the IXM-C to achieve full well coverage. Both systems were equipped with robotics to enable continuous imaging 24 hours/day. Cell segmentation was performed with Columbus (Perkin Elmer, Waltham, MA) or MetaXpress (Molecular Devices, San Jose, CA) depending on the system used for image acquisition. In both cases, nuclei were segmented based on their Hoechst signal, a ring was drawn around each nucleus, and the average intensity of each stain was measured in each mask. To account for local changes in background intensity, the ring intensity was subtracted from the nuclear intensity. The

average nuclear Hoechst intensity was multiplied by the nuclear area to obtain the DNA content measurement.

Validation of other antibodies and five channel Deep Dye Drop

Cells were seeded, treated and subjected to the Deep Dye Drop protocol as described above with the following modifications. Alternate antibodies were used in the place of pH3: actin (1:500, Cell Signaling Technologies, Danvers, MA), 53BP1 (1:500, BD Biosciences, Franklin Lakes, NJ), cytochrome C (1:200, Invitrogen, Carlsbad, CA), pRb (1:500, Cell Signaling Technologies, Danvers, MA). For five channel Deep Dye Drop, the protocol was followed as above, and cells were incubated overnight in the presence of pH3(S10) (1:2000, Cell Signaling Technologies, Danvers, MA) and 53BP1 (1:500, BD Biosciences, Franklin Lakes, NJ) primary antibodies. The cells were then washed and incubated with 1:2000 secondary donkey-anti-rabbit Alexa 488 and goat-anti-mouse Alexa 750 antibodies in Odyssey buffer for one hour at RT.

Cyclic immunofluorescence

MCF7 and MCF 10A cells were seeded 15,000 and 8000 cells per well in two 96 well plates (Corning, Glendale, AZ) and allowed to adhere for 24 h prior to treatment with ribociclib, BMS-265246 or DMSO for 72 h. Cells were then stained and fixed according to the Deep Dye Drop protocol, the click-chemistry EdU labeling step was omitted on plate one. Cells were then imaged, plate two was washed once with EDTA (10 mM in PBS), incubated at RT for 2 h. in 10 mM EDTA (60 µl/well) and washed three times with PBS. Both plates were then bleached for 1 h (60 µl per well of 3% (wt/vol) H_2O_2, 20 mM NaOH in PBS) exposed to light, washed three times with PBS and subjected to three rounds of cyclic immunofluorescence (see **Supplementary Table 4**).[33] Plate one was then bleached again, washed three times with PBS, and the EdU was labeled per the Deep Dye Drop protocol. Hoechst (1 µg/ml) was included in all staining rounds.

Data analysis

Analysis of the single cell level feature data was performed automatically with custom scripts (see Data and code availability below). The detailed computational protocol for gating measured signal intensities is available at https://github.com/datarail/DrugResponse/wiki. Briefly, The LDR, EdU, and pH3 intensities were log transformed and smoothed using a kernel density estimate (KDE) function. A peak finding algorithm was used to identify the global minima of the KDEs. The minima were used to set thresholds above which the cells were classified as dead (based on LDR), in S-phase (based on EdU) or in M-phase based on pH3 intensity. The integrated Hoechst intensity was used to quantify DNA content to discriminate between cells in the G1 and G2 phases of the cell cycle. Cells that were negative for EdU but had intermediate DNA content between thresholds set for G1 and G2 were classified as 'S dropout'. Cells positive for LDR but that no longer harbored any Hoechst signal were scored as 'corpses' and were included in the total dead cell count.

Standard GR, GR static, and GR toxic

Standard GR value are calculated as defined previously based on the number of viable cells (Hoechst positive and LDR negative).[16] Quantification of the cytostatic and cytotoxic components of the response relies on a simple model of population growth with live cells, x, growing exponentially at a doubling rate k_s while dead cells, d, are dying proportionally to x at a rate [$log(2)\ k_d$]. Consequently, the population model is ruled by the ODE system:

$$\frac{\mathrm{d}\, x(c,t)}{\mathrm{dt}} = \log(2) \cdot [k_s(c,t) - k_d(c,t)] \cdot x(t)$$

$$\frac{\mathrm{d}\, d(c,t)}{\mathrm{dt}} = \log(2)\ \cdot k_d(c,t) \cdot x(t)$$

Note that the term $\log(2)$ is a factor to convert doubling rate into growth rate and allows us to solve this ODE system for k_s and k_d as:

$$k_s(c,t) = \frac{1}{t} \cdot \left(1 + \frac{d(c,t)-d_0}{x(c,t)-x_0}\right) \cdot \log2\left(\frac{x(c,t)}{x_0}\right), \quad k_d(c,t) = \frac{1}{t} \cdot \frac{d(c,t)-d_0}{x(c,t)-x_0} \cdot \log2\left(\frac{x(c,t)}{x_0}\right),$$

Where:

- *x(c,t)* is the number of viable cells at time t at drug concentration c
- *d(c,t)* is the number of dead cells at time t at drug concentration c
- $x_0 = x(0,0)$, the number of live cells at the beginning of the treatment
- $d_0 = d(0,0)$, the number of dead cells at the beginning of the treatment

The rates $k_s(c,t)$ and $k_d(c,t)$ can be normalized by the untreated control rates and mapped to range of [0, 1] and, respectively, [-1, 0] defining $GR_s(c)$ and $GR_T(c)$ as:

$$GR_s(c) = 2^{gr_s(c)} - 1, \text{ where } gr_s(c) = \frac{k_s(c)}{k_s(0)} = \frac{\left(1 + \frac{d(c,t) - d_0}{x(c,t) - x_0}\right) \cdot \log2\left(\frac{x(c,t)}{x_0}\right)}{\left(1 + \frac{d(0,t) - d_0}{x(0,t) - x_0}\right) \cdot \log2\left(\frac{x(0,t)}{x_0}\right)}$$

And

$$GR_T(c) = 2^{gr_T(c)} - 1, \text{ where}$$
$$gr_T(c) = k_d(0) - k_d(c) = \frac{1}{t}\left[\left(\frac{d(0,t) - d_0}{x(0,t) - x_0}\right) \cdot \log2\left(\frac{x(0,t)}{x_0}\right) - \left(\frac{d(c,t) - d_0}{x(c,t) - x_0}\right) \cdot \log2\left(\frac{x(c,t)}{x_0}\right)\right]$$

Note that we set $d(c,t) - d_0$ to 1 if below 1 because dead cells are meant to be cumulative over the course of the experiment and that a numerical approximation based on a Taylor expansion is used if $x(c,t) \cong x_0$ (see code below).

GR values are related to GR_s and GR_T values as follows:

$$GR(c) = 2^{gr(c)} - 1, \text{ where } gr(c) = \frac{k_s(c) - k_d(c)}{k_s(0) - k_d(0)} \text{ and } k_{s/d} \text{ as above}$$

With the simplification of $k_d(0) = 0$:

$$(GR_s(c) + 1) \cdot (GR_T(c) + 1) = 2\text{^}[\, gr_s(c) + \ gr_T(c)\,] = 2\text{^}\left[\frac{k_s(c) - \ k_d(c) \cdot k_s(0)}{k_s(0)}\right]$$

Thus we can see that:

$(GR_s(c) + 1) \cdot (GR_T(c) + 1) \approx (GR(c) + 1)$ in cases where $k_d(c) \ll 0$ or $k_s(0) \ \cong 1$.

Gene set enrichment analysis in cell lines with extended S-phase duration

Gene expression data for TNBC cell lines in our study were downloaded from the Broad Cancer Cell Line Encyclopedia 21Q2 data release (https://depmap.org/portal/download/)[67]. Cell lines were separated into those with S phase longer than 20 h and all others. Cohen's d was used to measure the effect size for all genes. The 25 genes with the largest effect sizes were entered in Enrichr (https://maayanlab.cloud/Enrichr/)[68,69] to identify enriched Gene Ontology (GO) Molecular Function terms.

Data and code availability

GR, cell death, and cell cycle results for the breast cancer screening dataset presented in this paper are available for download from synapse (https://www.synapse.org/#!Synapse:syn26133007) and can be browsed online: https://labsyspharm.shinyapps.io/HMSLINCS_BRCA_Browser/. Detailed Dye Drop and Deep Dye Drop protocols are available on protocols.io: https://www.protocols.io/view/deep-dye-drop-protocol-96zh9f6. All scripts needed to analyze single cell intensity data are available on github: github.com/datarail/DrugResponse/tree/master/python/cell_cycle_gating and a user guide detailing installation of these tools and their execution is available online: https://ddd-gating.readthedocs.io/en/latest/index.html. The code needed for GR calculations is on github: github.com/datarail/gr_metrics. A web resource for calculating GR values and metrics is also available at grcalculator.org where additional information is available. The modularity of the suite of tools means that each component can be used independently of the others, or jointly depending on the experiment and equipment available. Refer to **Supplementary Fig. 6** for an overview of these resources and how the modules fit together.

ACKNOWLEDGEMENTS

We thank ICCB-L for assistance with compound management and drug treatments and Nathanael Gray for providing compounds. This work was funded by NIH grants U54-CA225088, U54-HL127365 and U24-DK116204 and a generous gift from the Termeer Foundation. We thank Michael P. Rout for fruitful discussion and the suggestion to use OptiPrep™ in developing the Dye Drop method.

OUTSIDE INTERESTS

PKS is a member of the SAB or BOD member of Applied Biomath, RareCyte Inc., and Glencoe Software; PKS is also a member of the NanoString and Montai Health SABs. In the last five years the Sorger lab has received research funding from Novartis and Merck. Sorger declares that none of these relationships have influenced the content of this manuscript. KS is currently an employee of Bristol Myers Squibb, MH and LG are currently employees of Genentech, and MN is currently an employee of Ribon Therapeutics. The other authors declare no outside interests.

REFERENCES

1. Barretina, J. *et al.* The Cancer Cell Line Encyclopedia enables predictive modelling of anticancer drug sensitivity. *Nature* **483**, 603–7 (2012).
2. Yang, W. *et al.* Genomics of Drug Sensitivity in Cancer (GDSC): a resource for therapeutic biomarker discovery in cancer cells. *Nucleic Acids Res.* **41**, D955–D961 (2013).
3. Huang, S. & Pang, L. Comparing statistical methods for quantifying drug sensitivity based on in vitro dose-response assays. *Assay Drug Dev. Technol.* **10**, 88–96 (2012).
4. Boutros, M., Heigwer, F. & Laufer, C. Microscopy-Based High-Content Screening. *Cell* **163**, 1314–1325 (2015).
5. Chan, G. K. Y., Kleinheinz, T. L., Peterson, D. & Moffat, J. G. A simple high-content cell cycle assay reveals frequent discrepancies between cell number and ATP and MTS proliferation assays. *PloS One* **8**, e63583 (2013).
6. Posimo, J. M. *et al.* Viability Assays for Cells in Culture. *J. Vis. Exp. JoVE* (2014) doi:10.3791/50645.
7. Mirzayans, R., Andrais, B. & Murray, D. Do Multiwell Plate High Throughput Assays Measure Loss of Cell Viability Following Exposure to Genotoxic Agents? *Int. J. Mol. Sci.* **18**, E1679 (2017).
8. Bickle, M. The beautiful cell: high-content screening in drug discovery. *Anal. Bioanal. Chem.* **398**, 219–226 (2010).
9. Bray, M. A. *et al.* Cell Painting, a high-content image-based assay for morphological profiling using multiplexed fluorescent dyes. *Nat Protoc* **11**, 1757–74 (2016).
10. Harris, L. A. *et al.* An unbiased metric of antiproliferative drug effect in vitro. *Nat Methods* **13**, 497–500 (2016).
11. Tian, C., Yang, C. & Spencer, S. L. EllipTrack: A Global-Local Cell-Tracking Pipeline for 2D Fluorescence Time-Lapse Microscopy. *Cell Rep.* **32**, 107984 (2020).
12. Mullard, A. Machine learning brings cell imaging promises into focus. *Nat. Rev. Drug Discov.* **18**, 653–655 (2019).
13. Bouhaddou, M. *et al.* Drug response consistency in CCLE and CGP. *Nature* **540**, E9–E10 (2016).
14. Haibe-Kains, B. *et al.* Inconsistency in large pharmacogenomic studies. *Nature* **504**, 389–393 (2013).
15. Niepel, M. *et al.* A Multi-center Study on the Reproducibility of Drug-Response Assays in Mammalian Cell Lines. *Cell Syst.* **9**, 35-48.e5 (2019).
16. Hafner, M., Niepel, M., Chung, M. & Sorger, P. K. Growth rate inhibition metrics correct for confounders in measuring sensitivity to cancer drugs. *Nat Methods* **13**, 521–7 (2016).
17. Auld, D. S. *et al.* Microplate Selection and Recommended Practices in High-throughput Screening and Quantitative Biology. in *Assay Guidance Manual* (eds. Markossian, S. et al.) (Eli Lilly & Company and the National Center for Advancing Translational Sciences, 2004).
18. Spencer, C. M. & Goa, K. L. Iodixanol. A review of its pharmacodynamic and pharmacokinetic properties and diagnostic use as an x-ray contrast medium. *Drugs* **52**, 899–927 (1996).
19. Hafner, M., Niepel, M., Chung, M. & Sorger, P. K. Growth rate inhibition metrics correct for confounders in measuring sensitivity to cancer drugs. *Nat Methods* **13**, 521–7 (2016).

20. Hafner, M., Niepel, M. & Sorger, P. K. Alternative drug sensitivity metrics improve preclinical cancer pharmacogenomics. *Nat. Biotechnol.* **35**, 500–502 (2017).
21. Lin, J.-R., Fallahi-Sichani, M. & Sorger, P. K. Highly multiplexed imaging of single cells using a high-throughput cyclic immunofluorescence method. *Nat. Commun.* **6**, 8390 (2015).
22. Mansoury, M., Hamed, M., Karmustaji, R., Al Hannan, F. & Safrany, S. T. The edge effect: A global problem. The trouble with culturing cells in 96-well plates. *Biochem. Biophys. Rep.* **26**, 100987 (2021).
23. Lundholt, B. K., Scudder, K. M. & Pagliaro, L. A simple technique for reducing edge effect in cell-based assays. *J. Biomol. Screen.* **8**, 566–570 (2003).
24. Walling, L., Carramanzana, N., Schulz, C., Romig, T. & Johnson, M. Mixing in 384-well plates: issues, measurements, and solutions. *Assay Drug Dev. Technol.* **5**, 265–275 (2007).
25. Hafner, M., Niepel, M., Subramanian, K. & Sorger, P. K. Designing Drug-Response Experiments and Quantifying their Results. *Curr Protoc Chem Biol* **9**, 96–116 (2017).
26. NIH CIT Consortium Chemistry Manufacturing Controls Monitoring Committee & NIH CIT Consortium. Raw Material Specification, OptiPrep. *CellR4-- Repair Replace. Regen. Reprogramming* **4**, (2016).
27. Mita, A. *et al.* Antiproinflammatory Effects of Iodixanol (OptiPrep)-Based Density Gradient Purification on Human Islet Preparations. *Cell Transplant.* **19**, 1537–1546 (2010).
28. Chan, L. L.-Y., McCulley, K. J. & Kessel, S. L. Assessment of Cell Viability with Single-, Dual-, and Multi-Staining Methods Using Image Cytometry. *Methods Mol. Biol. Clifton NJ* **1601**, 27–41 (2017).
29. Flow cytometric estimation of cell cycle parameters using a monoclonal antibody to bromodeoxyuridine - Sasaki - 1986 - Cytometry - Wiley Online Library. https://onlinelibrary.wiley.com/doi/abs/10.1002/cyto.990070415.
30. Romero-Pozuelo, J., Figlia, G., Kaya, O., Martin-Villalba, A. & Teleman, A. A. Cdk4 and Cdk6 Couple the Cell-Cycle Machinery to Cell Growth via mTORC1. *Cell Rep.* **31**, 107504 (2020).
31. Goel, S. *et al.* Overcoming Therapeutic Resistance in HER2-Positive Breast Cancers with CDK4/6 Inhibitors. *Cancer Cell* **29**, 255–69 (2016).
32. Cai, J., Yang, J. & Jones, DeanP. Mitochondrial control of apoptosis: the role of cytochrome c. *Biochim. Biophys. Acta BBA - Bioenerg.* **1366**, 139–149 (1998).
33. Lin, J.-R., Fallahi-Sichani, M. & Sorger, P. K. Highly multiplexed imaging of single cells using a high-throughput cyclic immunofluorescence method. *Nat. Commun.* **6**, 8390 (2015).
34. Shaffer, S. M. *et al.* Rare cell variability and drug-induced reprogramming as a mode of cancer drug resistance. *Nature* **546**, 431–435 (2017).
35. Burke, T. *et al.* Abstract 2830: The major human metabolites of abemaciclib are inhibitors of CDK4 and CDK6. *Cancer Res.* **76**, 2830–2830 (2016).
36. Patnaik, A. *et al.* Efficacy and Safety of Abemaciclib, an Inhibitor of CDK4 and CDK6, for Patients with Breast Cancer, Non–Small Cell Lung Cancer, and Other Solid Tumors. *Cancer Discov.* **6**, (2016).

37. Hafner, M. *et al.* Multiomics Profiling Establishes the Polypharmacology of FDA-Approved CDK4/6 Inhibitors and the Potential for Differential Clinical Activity. *Cell Chem. Biol.* **26**, 1067-1080.e8 (2019).
38. Herrera-Abreu, M. T. *et al.* Early Adaptation and Acquired Resistance to CDK4/6 Inhibition in Estrogen Receptor-Positive Breast Cancer. *Cancer Res.* **76**, 2301–2313 (2016).
39. Fallahi-Sichani, M., Honarnejad, S., Heiser, L. M., Gray, J. W. & Sorger, P. K. Metrics other than potency reveal systematic variation in responses to cancer drugs. *Nat. Chem. Biol.* **9**, 708–714 (2013).
40. Jang, I. S., Neto, E. C., Guinney, J., Friend, S. H. & Margolin, A. A. SYSTEMATIC ASSESSMENT OF ANALYTICAL METHODS FOR DRUG SENSITIVITY PREDICTION FROM CANCER CELL LINE DATA. *Pac. Symp. Biocomput. Pac. Symp. Biocomput.* 63–74 (2014).
41. Pozdeyev, N. *et al.* Integrating heterogeneous drug sensitivity data from cancer pharmacogenomic studies. *Oncotarget* **7**, 51619–51625 (2016).
42. Narayan, P. *et al.* FDA Approval Summary: Alpelisib Plus Fulvestrant for Patients with HR-positive, HER2-negative, PIK3CA-mutated, Advanced or Metastatic Breast Cancer. *Clin. Cancer Res.* **27**, 1842–1849 (2021).
43. Rabindran, S. K. *et al.* Antitumor Activity of HKI-272, an Orally Active, Irreversible Inhibitor of the HER-2 Tyrosine Kinase. *Cancer Res.* **64**, 3958–3965 (2004).
44. Jerusalem, G., Rorive, A. & Collignon, J. Use of mTOR inhibitors in the treatment of breast cancer: an evaluation of factors that influence patient outcomes. *Breast Cancer Targets Ther.* **6**, 43–57 (2014).
45. Martorana, F. *et al.* AKT Inhibitors: New Weapons in the Fight Against Breast Cancer? *Front. Pharmacol.* **12**, 662232 (2021).
46. Steelman, L. S. *et al.* The therapeutic potential of mTOR inhibitors in breast cancer. *Br. J. Clin. Pharmacol.* **82**, 1189–1212 (2016).
47. Ha, D.-H. *et al.* Antitumor effect of a WEE1 inhibitor and potentiation of olaparib sensitivity by DNA damage response modulation in triple-negative breast cancer. *Sci. Rep.* **10**, 9930 (2020).
48. Hafner, M. *et al.* Quantification of sensitivity and resistance of breast cancer cell lines to anti-cancer drugs using GR metrics. *Sci. Data* **4**, 170166 (2017).
49. Wong, K.-K. *et al.* A Phase I Study with Neratinib (HKI-272), an Irreversible Pan ErbB Receptor Tyrosine Kinase Inhibitor, in Patients with Solid Tumors. *Clin. Cancer Res.* **15**, 2552–2558 (2009).
50. Nikolai, B. C. *et al.* HER2 signaling drives DNA anabolism and proliferation through SRC-3 phosphorylation and E2F1-regulated genes. *Cancer Res.* **76**, 1463–1475 (2016).
51. Sakamoto, K. M. *et al.* Protacs: chimeric molecules that target proteins to the Skp1-Cullin-F box complex for ubiquitination and degradation. *Proc. Natl. Acad. Sci. U. S. A.* **98**, 8554–8559 (2001).
52. Jiang, B. *et al.* Development of Dual and Selective Degraders of Cyclin-Dependent Kinases 4 and 6. *Angew. Chem. Int. Ed.* **58**, 6321–6326 (2019).
53. Brand, M. *et al.* Homolog-Selective Degradation as a Strategy to Probe the Function of CDK6 in AML. *Cell Chem. Biol.* **26**, 300-306.e9 (2019).

54. Chong, Q.-Y. *et al.* A unique CDK4/6 inhibitor: Current and future therapeutic strategies of abemaciclib. *Pharmacol. Res.* **156**, 104686 (2020).
55. Cai, D., Latham, V. M., Zhang, X. & Shapiro, G. I. Combined Depletion of Cell Cycle and Transcriptional Cyclin-Dependent Kinase Activities Induces Apoptosis in Cancer Cells. *Cancer Res.* **66**, 9270–9280 (2006).
56. Ubhi, T. & Brown, G. W. Exploiting DNA Replication Stress for Cancer Treatment. *Cancer Res.* **79**, 1730–1739 (2019).
57. Spasojevic, C. *et al.* PKD1 is a potential biomarker and therapeutic target in triple-negative breast cancer. *Oncotarget* **9**, 23208–23219 (2018).
58. Xiao, Y.-S. *et al.* Major vault protein is a direct target of Notch1 signaling and contributes to chemoresistance in triple-negative breast cancer cells. *Cancer Lett.* **440–441**, 156–167 (2019).
59. Pohl, S.-G. *et al.* Wnt signaling in triple-negative breast cancer. *Oncogenesis* **6**, e310–e310 (2017).
60. Wang, S., Liang, Y., Chang, W., Hu, B. & Zhang, Y. Triple Negative Breast Cancer Depends on Sphingosine Kinase 1 (SphK1)/Sphingosine-1-Phosphate (S1P)/Sphingosine 1-Phosphate Receptor 3 (S1PR3)/Notch Signaling for Metastasis. *Med. Sci. Monit. Int. Med. J. Exp. Clin. Res.* **24**, 1912–1923 (2018).
61. Choi, H. *et al.* CDK12 drives breast tumor initiation and trastuzumab resistance via WNT and IRS1-ErbB-PI3K signaling. *EMBO Rep.* **20**, e48058 (2019).
62. Lin, J.-R. *et al.* Highly multiplexed immunofluorescence imaging of human tissues and tumors using t-CyCIF and conventional optical microscopes. *eLife* **7**, e31657 (2018).
63. Hafner, M., Niepel, M., Chung, M. & Sorger, P. K. Growth rate inhibition metrics correct for confounders in measuring sensitivity to cancer drugs. *Nat. Methods* **13**, 521–527 (2016).
64. Hafner, M. *et al.* Multiomics Profiling Establishes the Polypharmacology of FDA-Approved CDK4/6 Inhibitors and the Potential for Differential Clinical Activity. *Cell Chem. Biol.* **26**, 1067-1080.e8 (2019).
65. Wander, S. A. *et al.* A multicenter analysis of abemaciclib after progression on palbociclib in patients (pts) with hormone receptor-positive (HR+)/HER2- metastatic breast cancer (MBC). *J. Clin. Oncol.* **37**, 1057–1057 (2019).
66. Wiernik, P. H. Alvocidib (flavopiridol) for the treatment of chronic lymphocytic leukemia. *Expert Opin. Investig. Drugs* **25**, 729–734 (2016).
67. Tsherniak, A. *et al.* Defining a Cancer Dependency Map. *Cell* **170**, 564-576.e16 (2017).
68. Chen, E. Y. *et al.* Enrichr: interactive and collaborative HTML5 gene list enrichment analysis tool. *BMC Bioinformatics* **14**, 128 (2013).
69. Kuleshov, M. V. *et al.* Enrichr: a comprehensive gene set enrichment analysis web server 2016 update. *Nucleic Acids Res.* **44**, W90–W97 (2016).

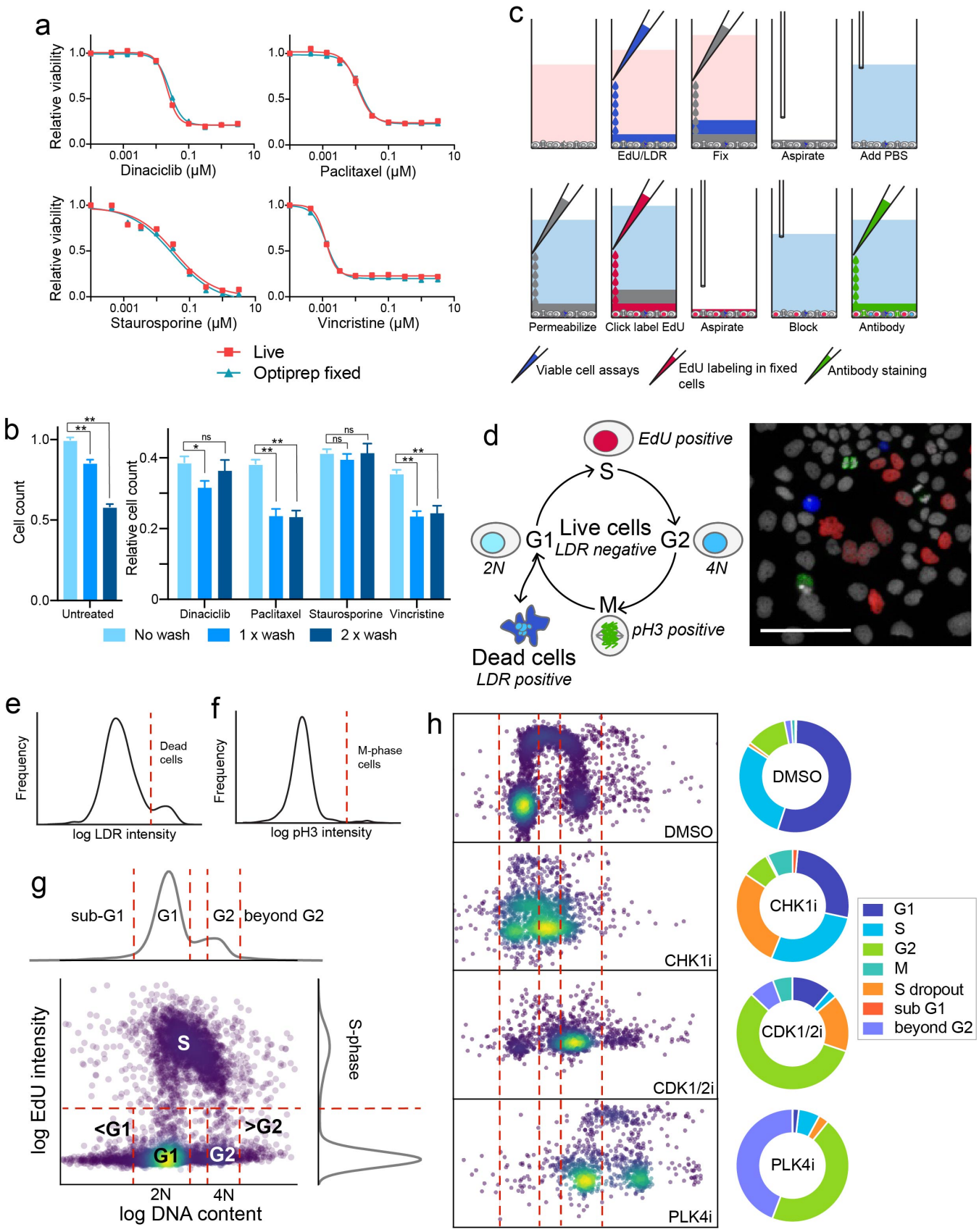
a
Relative viability
Dinaciclib (μM)
Paclitaxel (μM)
Staurosporine (μM)
Vincristine (μM)
Live
Optiprep fixed
b
Cell count
Relative cell count
Untreated
Dinaciclib
Paclitaxel
Staurosporine
Vincristine
No wash
1 x wash
2 x wash
c
EdU/LDR
Fix
Aspirate
Add PBS
Permeabilize
Click label EdU
Block
Antibody
Viable cell assays
EdU labeling in fixed cells
Antibody staining
d
EdU positive
S
Live cells
LDR negative
G1
G2
2N
4N
M
pH3 positive
Dead cells
LDR positive
e
Frequency
Dead cells
log LDR intensity
f
M-phase cells
log pH3 intensity
g
sub-G1
G1
G2
beyond G2
log EdU intensity
S
<G1
>G2
G1
G2
S-phase
2N
4N
log DNA content
h
DMSO
CHK1i
CDK1/2i
PLK4i
G1
S
G2
M
S dropout
sub G1
beyond G2

Figure 1: Sequential density-based staining and fixation prevent cell loss from multi-well plates (a) Relative cell viability in OptiPrep™ fixed cells as compared to live cell microscopy following 24 h treatments with increasing concentrations of dinaciclib, paclitaxel, staurosporine, and vincristine in MCF 10A-H2B-mCherry cells. Error bars represent the standard error of the mean of eight technical replicates from one representative biological replicate. (b) Consequences of one or two wash cycles prior to fixation on MCF 10A-H2B-mCherry cells untreated and treated with 0.1 μM dinaciclib, paclitaxel, staurosporine, and vincristine for 24 h. Error bars represent the standard error of the mean of eight technical replicates from one representative biological replicate, ** indicates P-value < 0.001, * indicates P-value < 0.01, ns indicates not significantly different by 2-way ANOVA with Dunnett's multiple comparison test. (c) Deep Dye Drop protocol steps: EdU and LDR dye are added in 10% OptiPrep™ followed by fixation with 4% formaldehyde in 20% Optiprep™. Cells are then permeabilized with 0.5% Triton X-100 in 10% OptiPrep, and the EdU is labeled with a fluorescent dye azide via Click chemistry in 20% OptiPrep™. The contents of the well are aspirated, cells are blocked, and then stained with a conjugated antibody against phospho-histone H3 (pH3) in 10% OptiPrep™. One well of a multi-well plate is depicted. (d) Schematic and representative image of cells stained with the Deep Dye Drop protocol. Nuclei are stained with Hoechst (gray-scale), dead cells are stained with LIVE/DEAD red (blue), S-phase cells are labeled with EdU (red) and M-phase cells are stained with phospho-histone H3 (green). (e) Thresholds set to classify dead cells shown on a distribution of LDR intensity values and (f) to identify cells in M-phase shown on a distribution of pH3 intensity values. (g) Scatter plot of EdU intensity versus DNA content. The red dotted lines represent gating applied to assign cells to the sub G1, G1, G2, beyond G2, and S-phases of the cell cycle (see online Methods). (h) DNA content in BT20 cells treated for 72 hours with inhibitors targeting CHK1 (1 μM LY2606368), CDK1/2 (3.16 μM BMS-265246) and PLK4 (0.316 μM CFI-400495) and untreated controls.

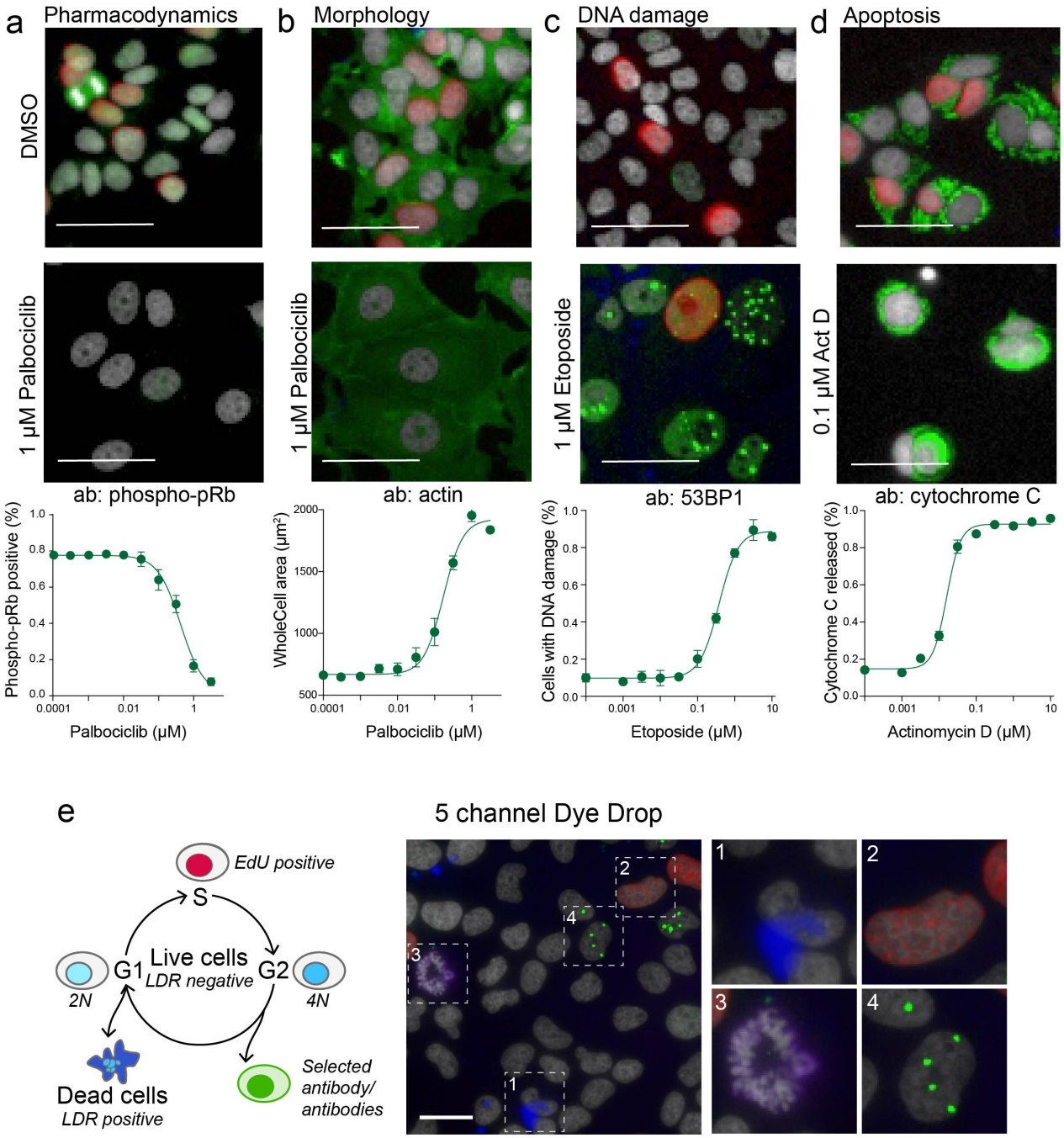

Figure 2: Customization of antibody incorporation in Dye Drop assays (a) MCF7 cells stained with phospho-pRb and (b) actin untreated and after 72 h in 1 µM palbociclib; effects of increasing concentrations of palbociclib on the fraction of phospho-pRb positive MCF7 cells, or (b) on cell size as detected with actin staining after 72 h. (c) MCF 10A cells stained with 53BP1 untreated and after 72 h in 1 µM etoposide; induction of DNA damage by increasing concentrations of etoposide in MCF 10A cells as detected with 53BP1 staining after 72 h. (d) MCF7 cells stained with cytochrome C untreated and after 72 h in 0.1 µM actinomycin D; effect of increasing concentrations of actinomycin D on release of cytochrome C from the mitochondria in MCF7 cells after 72 h, performed in duplicate. Nuclei are stained with Hoechst (gray-scale), and EdU (red) in all images. Error bars represent the standard deviation of the mean of four replicates unless otherwise specified. Scale bars are 50 µm. (e) Schematic and representative image of the addition of a fifth channel to the Deep Dye Drop assay: cells are stained with Hoechst (gray-scale), LDR (blue, 1), EdU (red, 2), pH3 (purple, 3) and 53BP1 (green, 4).

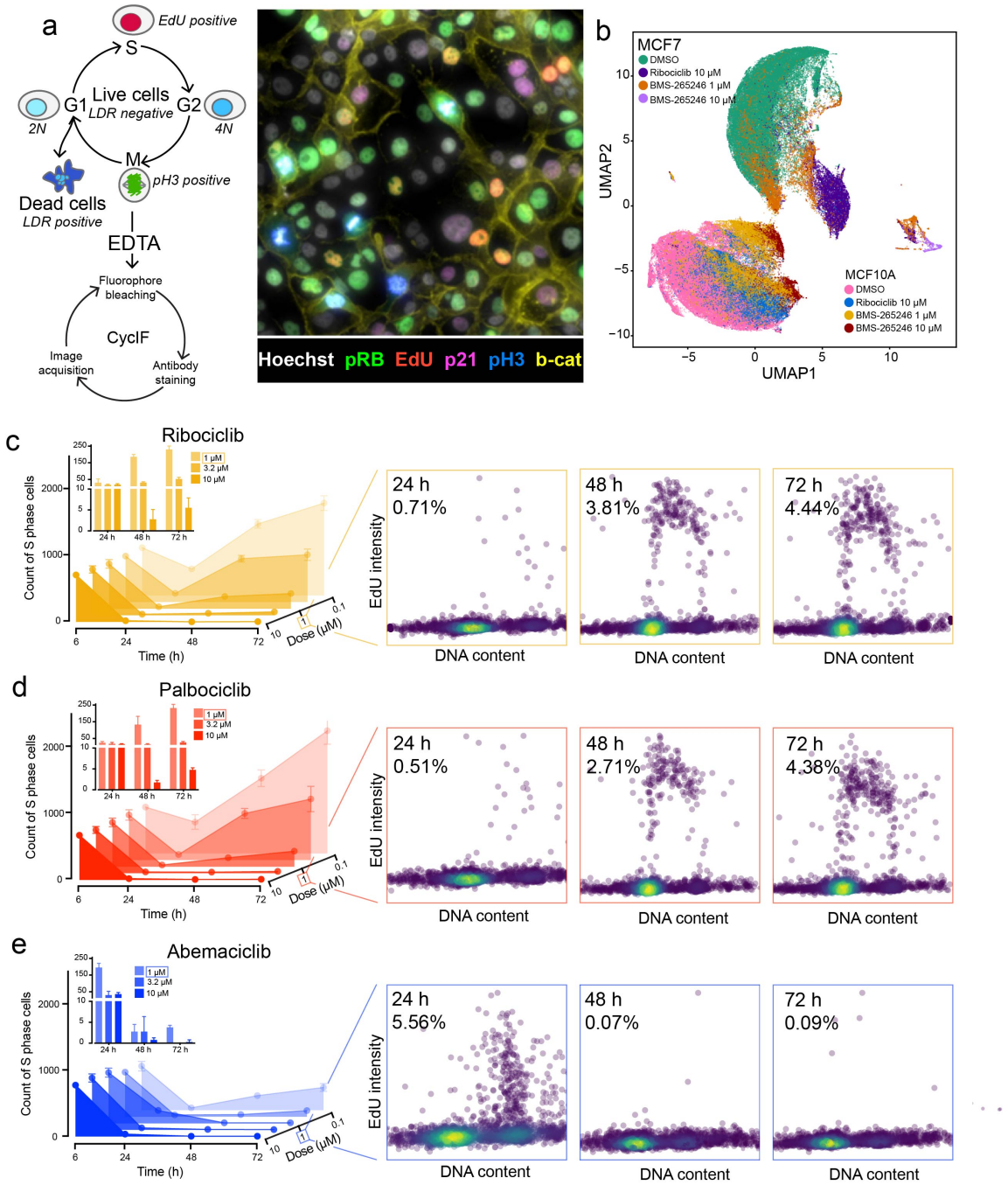

Figure 3: Integration of Dye Drop assays with CyCIF and time series (a) Schematic and representative image of multiplexing Deep Dye Drop assays with cyclic immunofluorescence: the Hoechst (gray-scale), EdU (red), pH3 (green), beta-catenin (cyan), phospho-pRb (blue), and p21 (yellow) signals are displayed. (b) UMAP representation of MCF7 and MCF 10A cells treated with BMS-265246 (1 μM, 10 μM), ribociclib (10 μM) or DMSO stained with Deep Dye Drop and cyclic immunofluorescence. (c) The number of MCF7 cells in S-phase following treatment with increasing concentrations of ribociclib, (d) palbociclib, and (e) abemaciclib after 6, 24, 48, and 72 h. EdU versus DNA content scatter plots show the single cell cell-cycle distribution at 1 μM doses of each drug at the time points indicated, the percentage of cells in S-phase is indicated on each plot. Error bars represent the standard deviation of four technical replicates.

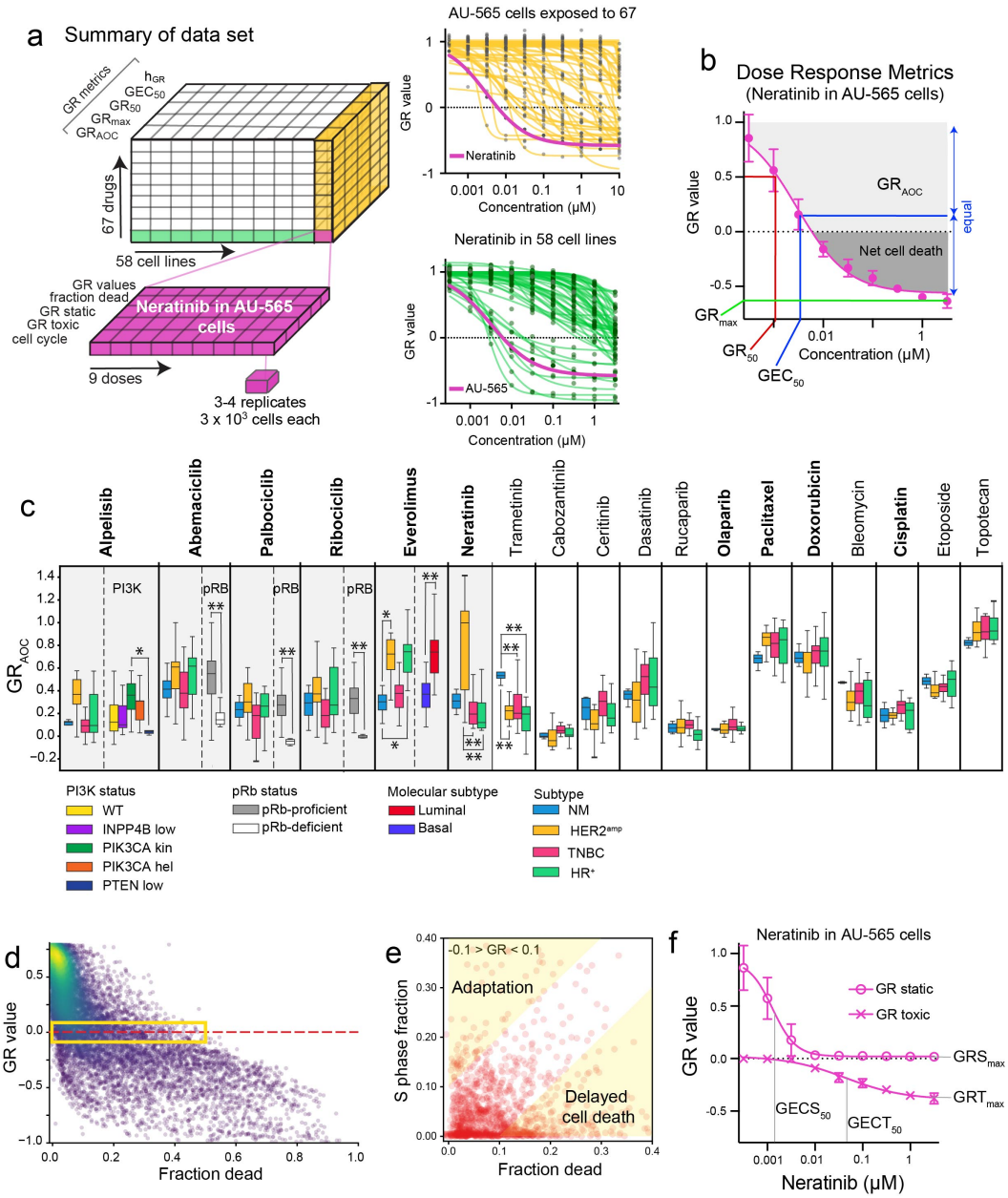

Figure 4: Dye Drop screening of a breast cancer cell line panel treated with a kinase inhibitor library (a) Dye Drop and Deep Dye Drop assays were used to measure the responses of 58 breast cancer cell lines treated with 67 drugs at nine concentrations after 72 h in technical triplicate or quadruplicate. GR-dose response curves for all drugs in AU-565 cells and all cell lines treated with neratinib. The response of AU-565 cells to neratinib is shown in pink. Error bars are omitted for simplicity. (b) Illustration of GR metrics shown on the neratinib-AU-565 dose response curve. (c) Box plot of GR_{AOC} values for FDA-approved drugs included in our screen. Cell lines are separated by clinical subtype, the bar within each box represents the median value and error bars represent the range of values. * P-value < 0.05, ** P-value < 0.01, 2-way ANOVA with Tukey's correction for multiple comparisons, or unpaired 2-tailed t-test. The shaded region indicates responses that align with known biomarkers. (d) Variability in fraction dead with respect to GR value for all dose response data, GR values > 0.8 are not shown. (e) Fraction of cells in S phase relative to fraction dead for conditions resulting in -0.1 > GR < 0.1. Regions indicative of late-onset cell death and adaptation to drug are highlighted in yellow. (f) GR^S and GR^T curves for AU-565 cells treated with neratinib. Error bars represent the standard deviation of technical quadruplicates.

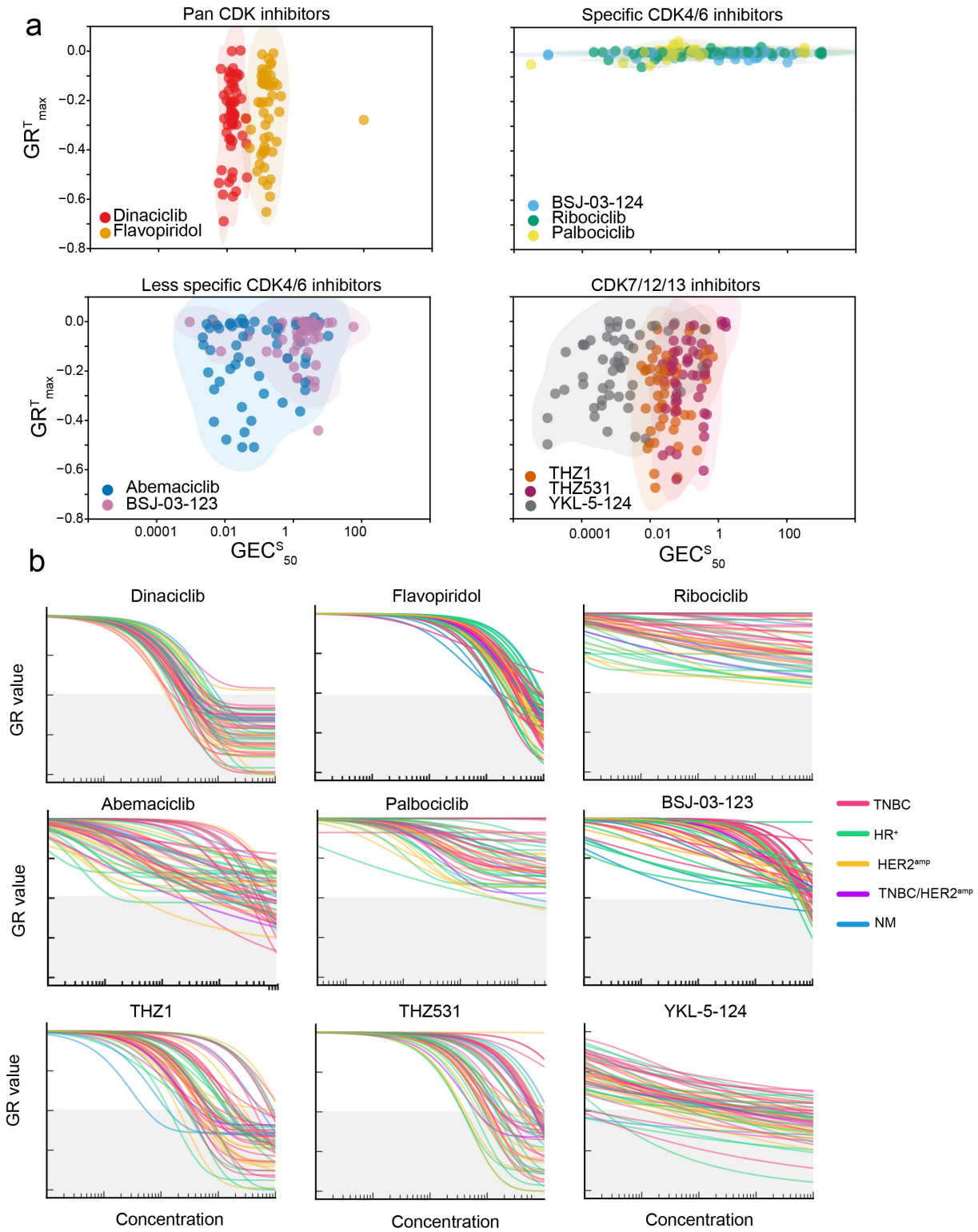

Figure 5: Variation in static and toxic components of responses to CDK inhibitors (a) Relationship between GR^{T}_{max} and GEC^{S}_{50} for drugs targeting pan-CDKs (top-left), CDK4/6 (top-right), CDK4/6 and off-targets (bottom-left) and CDK7/12/13 (bottom-right). Shading is for visualization only. (b) The dose response curves for the same conditions shown in (a) 72 h after drug addition.

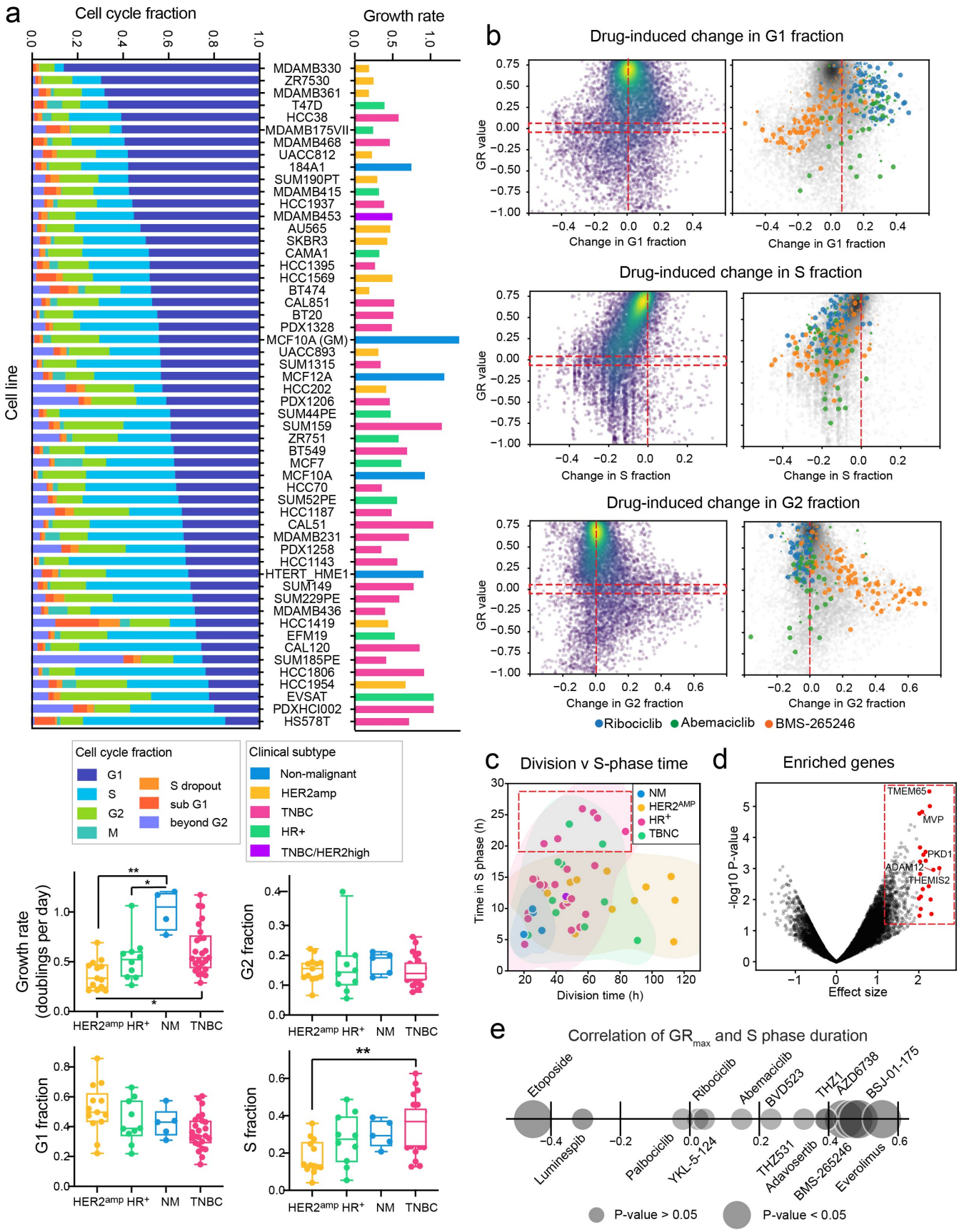
a
Cell cycle fraction
Growth rate
Cell line
MDAMB330
ZR7530
MDAMB361
T47D
HCC38
MDAMB175VII
MDAMB468
UACC812
184A1
SUM190PT
MDAMB415
HCC1937
MDAMB453
AU565
SKBR3
CAMA1
HCC1395
HCC1569
BT474
CAL851
BT20
PDX1328
MCF10A (GM)
UACC893
SUM1315
MCF12A
HCC202
PDX1206
SUM44PE
SUM159
ZR751
BT549
MCF7
MCF10A
HCC70
SUM52PE
HCC1187
CAL51
MDAMB231
PDX1258
HCC1143
HTERT_HME1
SUM149
SUM229PE
MDAMB436
HCC1419
EFM19
CAL120
SUM185PE
HCC1806
HCC1954
EVSAT
PDXHCI002
HS578T
Cell cycle fraction
G1
S
G2
M
S dropout
sub G1
beyond G2
Clinical subtype
Non-malignant
HER2amp
TNBC
HR+
TNBC/HER2high
Growth rate (doublings per day)
G2 fraction
G1 fraction
S fraction
HER2amp
HR+
NM
TNBC
b
Drug-induced change in G1 fraction
Drug-induced change in S fraction
Drug-induced change in G2 fraction
GR value
Change in G1 fraction
Change in S fraction
Change in G2 fraction
Ribociclib
Abemaciclib
BMS-265246
c
Division v S-phase time
NM
HER2AMP
HR+
TBNC
Time in S phase (h)
Division time (h)
d
Enriched genes
TMEM65
MVP
PKD1
ADAM12
THEMIS2
-log10 P-value
Effect size
e
Correlation of GRmax and S phase duration
Etoposide
Ribociclib
Abemaciclib
BVD523
THZ1
AZD6738
BSJ-01-175
Luminespib
Palbociclib
YKL-5-124
THZ531
Adavosertib
BMS-265246
Everolimus
P-value > 0.05
P-value < 0.05

Figure 6: Cell cycle at baseline and in response to drug treatment (a) The baseline distribution throughout the cell cycle phases and growth rate in doublings per day for 58 breast cancer cell lines. Boxplots of the growth rate, and the fraction of cells at baseline in the G1, G2, and S phases of the cell cycle for the same cell lines separated by clinical subtype. All cell lines were pulsed with EdU for 1 h to identify those in S-phase. (b) Drug-induced change (compared to DMSO control) in the G1, S and G2 fractions with respect to GR value for all dose response data (left panels) and highlighted for ribociclib, abemaciclib and BMS-265246 (right panels). The size of the data point represents dose. (c) Duration of S-phase with respect to division time for 58 breast cancer cell lines, colored by clinical subtype. The dashed red box indicates S-phase duration > 20 h. (d) Genes enriched in TNBC cells with S phases > 20 h relative to those with shorter S-phases. The 25 genes with the largest effect sizes are highlighted in red. (e) Spearman correlation between the duration of S-phase and the GRmax of the dose response curves across all cell lines for the drugs indicated.

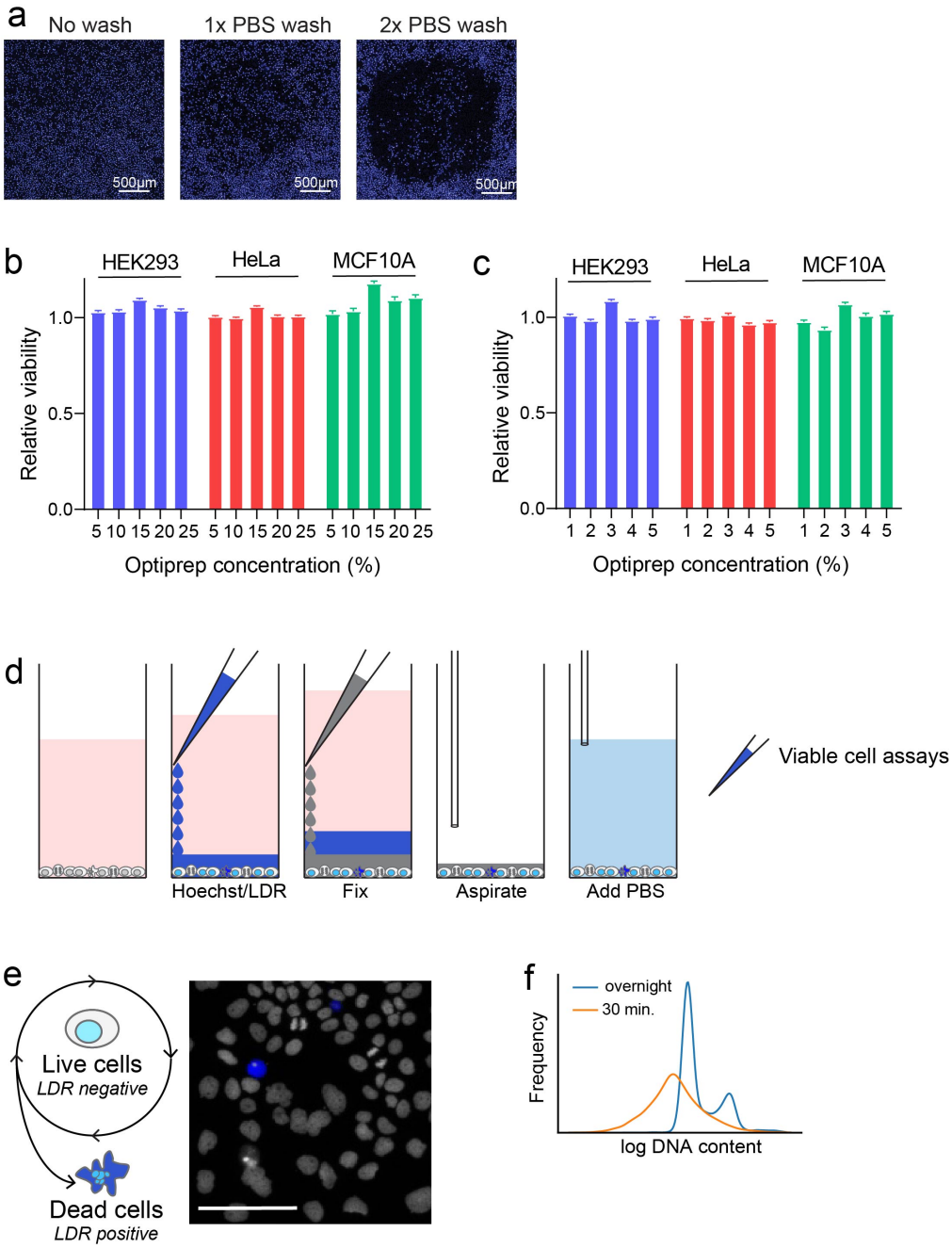

Supplementary Figure 1: Validation of assay conditions and assay schematics (a) Images of cells in a well of a 384 well plate stained with Hoechst in OptiPrep™ without prior washing and following one or two PBS wash cycles with a robotic plate washer. (b) Effects of a one hour pulse of increasing concentrations of OptiPrep™ on the viability of HEK293, HeLa and MCF 10A cells 24 h later. Error bars represent standard error of the mean. (c) Effects of a 24 h exposure to increasing concentrations of OptiPrep™ on the viability of HEK293, HeLa and MCF 10A cells. (d) Dye Drop protocol steps: Hoechst and LIVE/DEAD (LDR) dye are added in 10% OptiPrep™ followed by 4% formaldehyde in 20% OptiPrep™, the contents of the well are aspirated, and replaced with PBS. One well of a multi-well plate is depicted. (e) Schematic of Dye Drop staining and image showing cells stained with the Dye Drop protocol. Hoechst staining is gray-scale and LDR staining is blue. (f) DNA content quantified from untreated BT20 cells stained with the Dye Drop (Hoechst 30 min) and Deep Dye Drop (Hoechst overnight (o/n)) protocols.

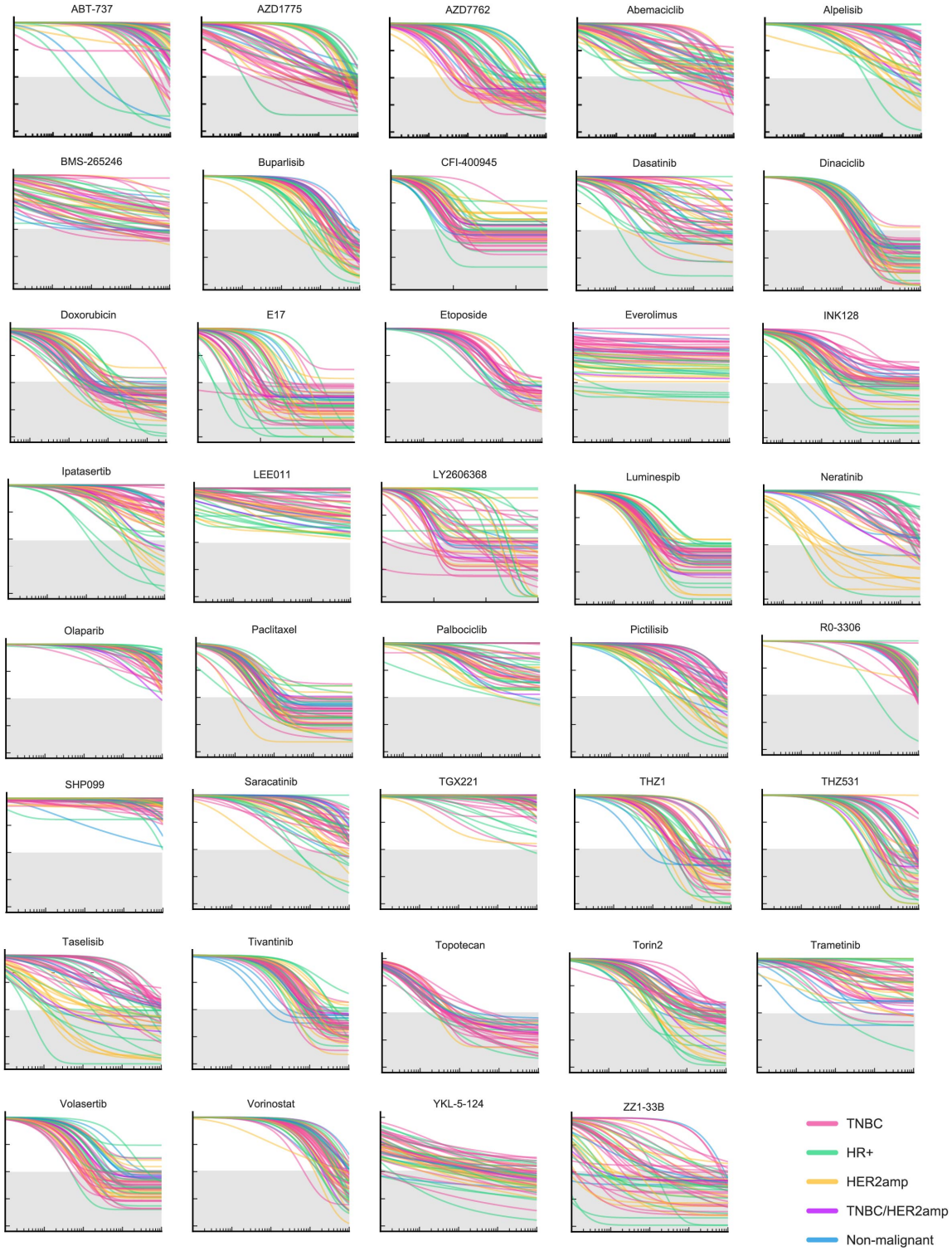

Supplementary Figure 2: GR dose response curves for select drugs in 58 cell lines GR-based dose response curves for 58 breast cancer cell lines treated with increasing concentrations of the drugs indicated for 72 hours. Cells were either stained with the Dye Drop or Deep Dye Drop assays. Each curve represents the fit to the average of three or four technical replicates, error bars are not shown for visual simplicity. Curves are colored by clinical subtype.

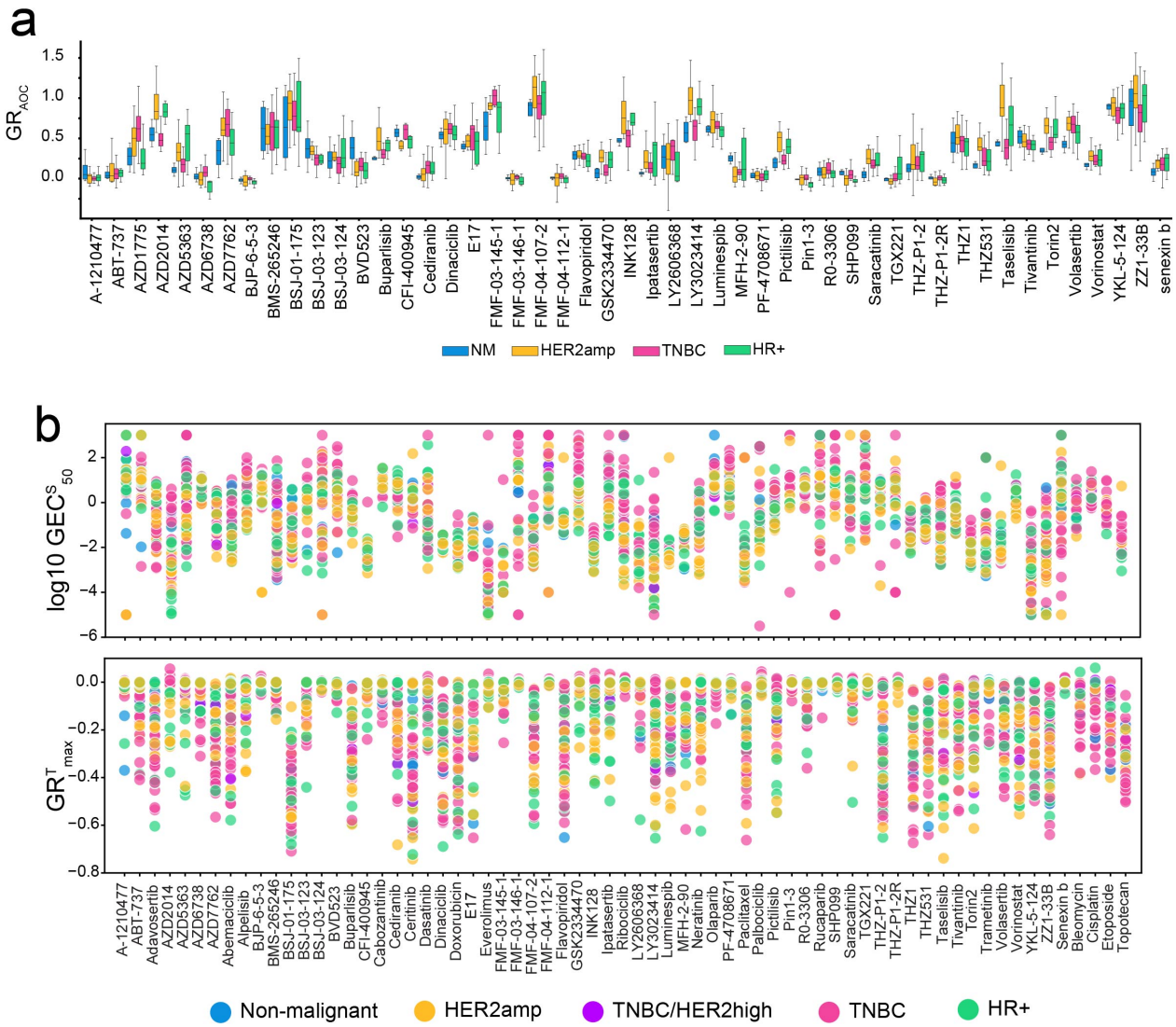

Supplementary Figure 3: GR metrics definitions and results for 67 drugs in 58 breast cancer cell lines (a) Area over the GR curves for the responses of non-FDA-approved drugs screened in 58 cell lines colored by clinical subtype. (b) GECS50 and (e) GRTmax metrics for 67 drugs in 58 breast cancer cell lines.

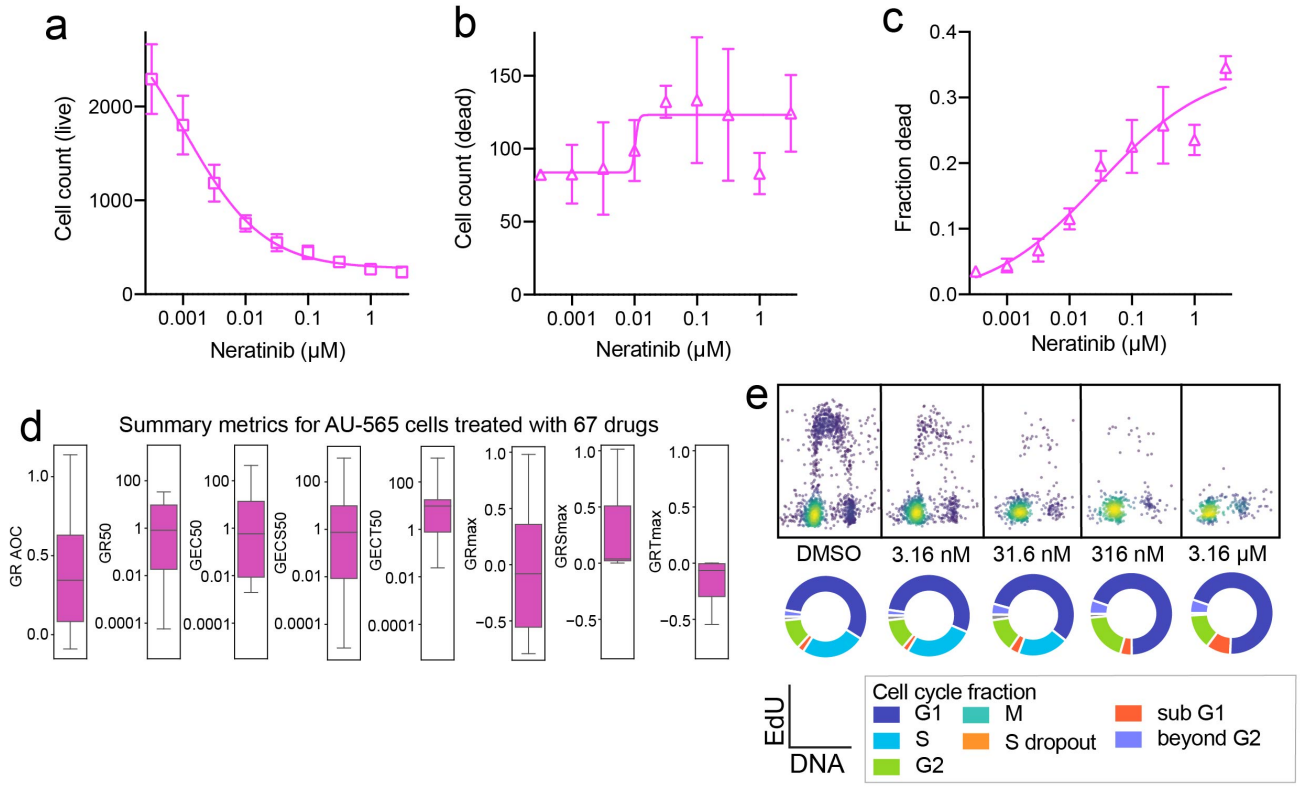

Supplementary Figure 4: Neratinib response in AU-565 cells (a) Live cell counts, (b) dead cell counts and (c) fraction of cells that are dead in AU-565 cells treated with neratinib at increasing concentrations for 72 h. (d) GR metrics across 58 breast cancer cell lines treated with neratinib. (e) Single cell EdU vs DNA content plots for the same conditions at the concentrations indicated with corresponding circular cell cycle fraction charts.

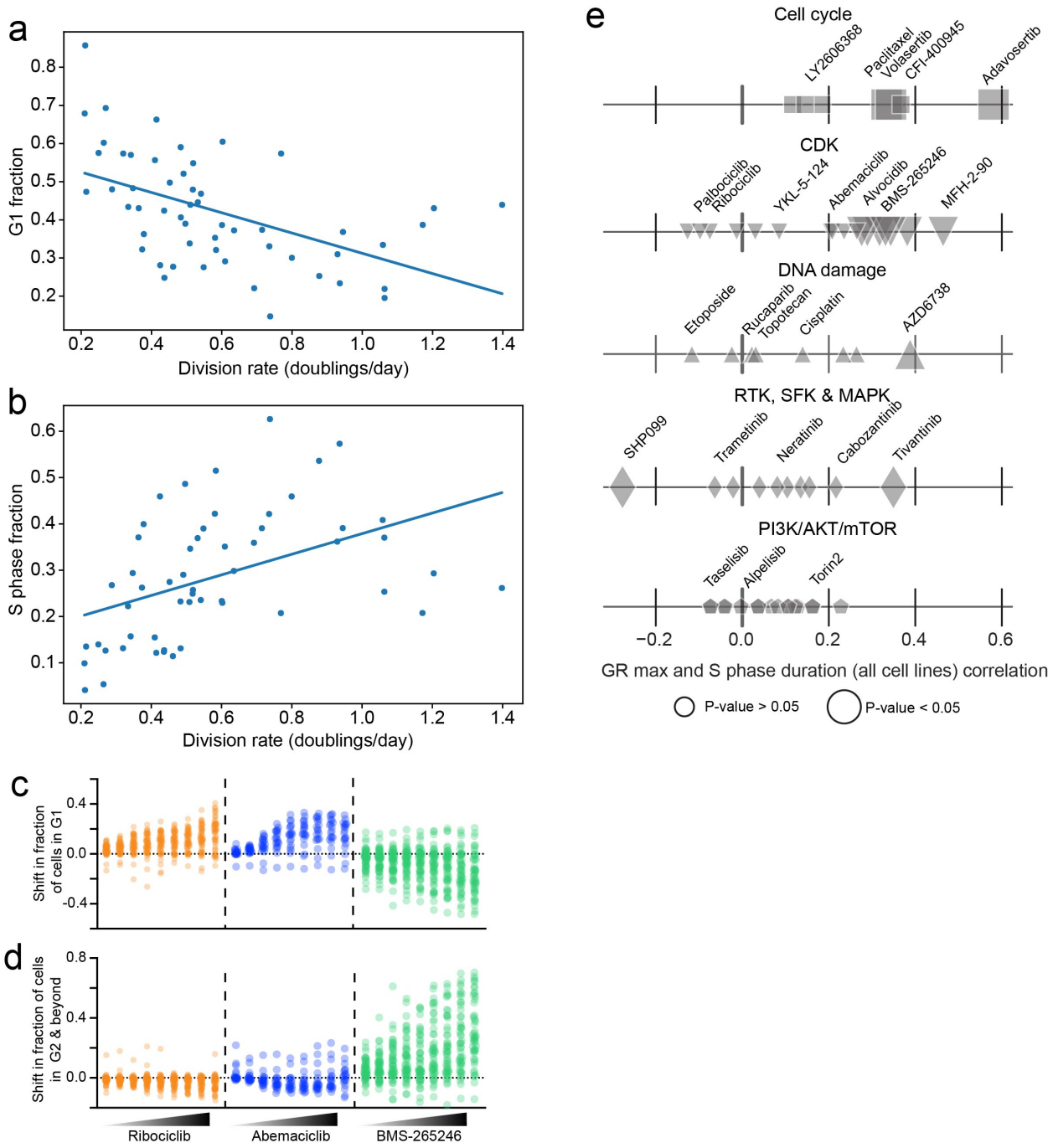

Supplementary Figure 5: Relationship between baseline cell cycle distribution and drug response (a) G1 and (b) S phase fraction with respect to division rate for 58 breast cancer cell lines. (c) The effects of increasing concentrations of ribociclib, abemaciclib and BMS-265246 on the fraction of cells in G1, and (d) in G2 or with DNA content in excess of G2. (e) Spearman correlation between the duration of S-phase and the GRmax of the dose response curves across all cell lines for all drugs tested organized by pathway targeted.

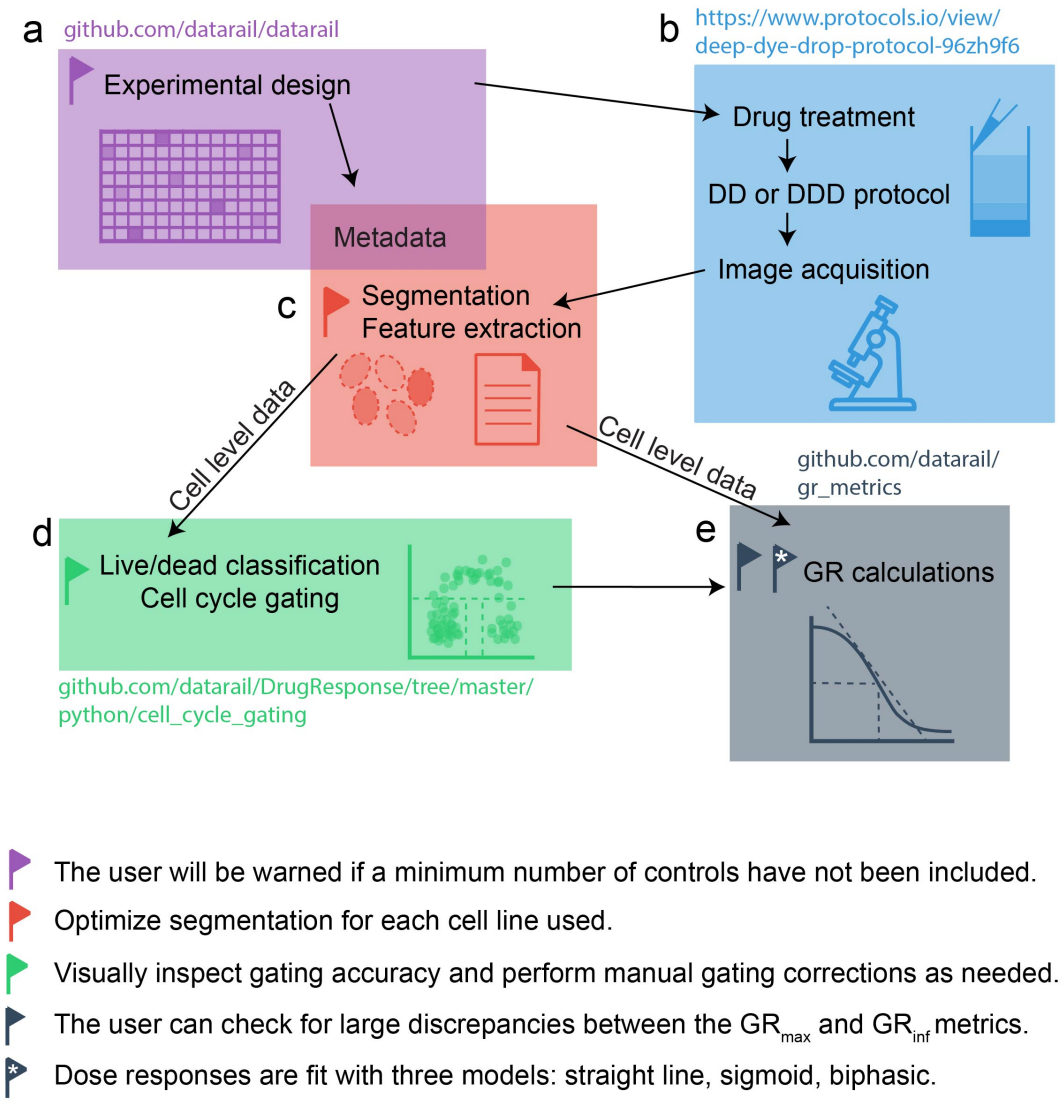

The user will be warned if a minimum number of controls have not been included.

Optimize segmentation for each cell line used.

Visually inspect gating accuracy and perform manual gating corrections as needed.

The user can check for large discrepancies between the GR_{max} and GR_{inf} metrics.

Dose responses are fit with three models: straight line, sigmoid, biphasic.

Supplementary Figure 6: Overview of the components of a dose response experiment and available tools (a) Automated experimental design Jupyter notebook for the randomization of dose response studies in multi-well plates. User input: experimental parameters (drugs, concentrations, time points, cell lines etc.); output: treatment file for a D300 digital drug dispenser and the associated metadata. The user is alerted if their experimental design does not include sufficient control wells (set at 8 per cell line). (b) Following drug treatment, cells are stained and fixed using the Dye Drop (DD) or Deep Dye Drop (DDD) assay, and images are acquired on any high throughput microscope. (c) Segmentation and feature extraction are performed and merged with the metadata. (d) Single cell level data can be gated automatically into the phases of the cell cycle. The user is presented with the gates overlaid on EdU versus DNA content scatter plots for visual inspection; should the gating be inaccurate it can be manually adjusted. Users have the option of having gates defined on negative control wells applied to treated wells, or of gating each well independently. (e) Well level data, either from feature extraction software, or summarized from single cell gating, are used to calculate GR values and fit GR metrics either using the online calculator (grcalculator.org), or a Jupyter notebook. (f) Stacked bar graphs for cell cycle, dose response curves (GR values, GR static, GR toxic and fraction dead), and summary metrics (per drug - cell line pair for each timepoint) are output. The suite of tools is modular, each component can be used independently of the others, or jointly depending on the experiment and equipment available.